



The resolution to the problem of consistent large transverse momentum in TMDs

J. O. Gonzalez-Hernandez *

*Dipartimento di Fisica, Università degli Studi di Torino, Via P. Giuria 1, I-10125, Torino, Italy and
INFN, Sezione di Torino, Via P. Giuria 1, Torino, I-10125, Italy*

T. Rainaldi [†] and T. C. Rogers [‡]

*Department of Physics, Old Dominion University, Norfolk, VA 23529, USA and
Jefferson Lab, 12000 Jefferson Avenue, Newport News, VA 23606, USA*

(Dated: March 10, 2023)

Parametrizing TMD parton densities and fragmentation functions in ways that consistently match their large transverse momentum behavior in standard collinear factorization has remained notoriously difficult. We show how the problem is solved in a recently introduced set of steps for combining perturbative and nonperturbative transverse momentum in TMD factorization. Called a “bottom-up” approach in a previous article, here we call it a “hadron structure oriented” (HSO) approach to emphasize its focus on preserving a connection to the TMD parton model interpretation. We show that the associated consistency constraints improve considerably the agreement between parametrizations of TMD functions and their large- k_T behavior, as calculated in collinear factorization. The procedure discussed herein will be important for guiding future extractions of TMD parton densities and fragmentation functions and for testing TMD factorization and universality. We illustrate the procedure with an application to semi-inclusive deep inelastic scattering (SIDIS) structure functions at an input scale Q_0 , and we show that there is improved consistency between different methods of calculating at moderate transverse momentum. We end with a discussion of plans for future phenomenological applications.

I. INTRODUCTION

Transverse momentum dependent (TMD) parton distribution functions (pdfs) and/or fragmentation functions (ffs), together with the TMD factorization theorems [1–3], have acquired a wide range of applications in hadronic, nuclear and high energy phenomenology [4, 5] over the past few decades. They are useful both for studying the role of intrinsic or nonperturbative effects in hadrons [6, 7] and for predicting transverse momentum distributions in cross sections after evolution to high energies. In the former case, they play an important role in testing, and thus refining, the partonic constituent interpretation of hadron structure. However, separating truly nonperturbative or intrinsic transverse momentum effects from the perturbatively generated transverse momentum that is calculable with collinear factorization has remained a difficult challenge. It is a problem that limits the predictive power of TMD factorization and creates ambiguity about the interpretation of phenomenologically extracted nonperturbative objects. This is especially the case with lower invariant energies, near the boundary between what may be considered an appropriate hard scale.

To see the issues clearly, recall that one normally categorizes contributions to a TMD cross section, such as semi-inclusive deep inelastic scattering (SIDIS), according to its transverse momentum regions. On one hand, the small transverse momentum regions are associated with nonperturbative effects in hadronic bound states. There, purely nonperturbative parton model descriptions are often quite successful phenomenologically, especially for moderate Q . On the other hand, in the regions of large q_T perturbative tails where $q_T \approx Q$, calculations can be performed in fixed order perturbation theory with collinear factorization with Q as a hard scale. One example of this way of cataloging physically distinct regions can be seen in the treatment of SIDIS in Ref. [8], following the theoretical work in Ref. [9], where Fig. 17 shows two separate fits for the small transverse momentum nonperturbative peak and the large transverse momentum perturbative tail. Reference [8] attributes the behavior in each region to a different underlying physical mechanism, namely a nonperturbative peak and a perturbative tail at small and large transverse momentum respectively. There one reads that “the two exponential functions in our parameterisation F_1 can be attributed to two completely different underlying physics mechanisms that overlap in the region $P_{hT} \simeq 1.0 (\text{GeV}/c)^2$.”

*Electronic address: joseosvaldo.gonzalezhernandez@unito.it

[†]Electronic address: train005@odu.edu

[‡]Electronic address: trogers@odu.edu

Individual TMD pdfs and ffs can be viewed in an analogous way. When the transverse momentum in an individual TMD pdf is comparable to the renormalization scale μ , $k_T \approx \mu \approx \sqrt{\zeta}$, it is straightforward to calculate the TMD pdf directly from its operator definition at a fixed, low order in collinear factorization. This provides a very useful consistency check in phenomenological implementations. Namely, the parametrizations of TMD pdfs and ffs that are used in phenomenology must, within perturbative or power-suppressed errors, match their expressions as obtained from fixed order collinear factorization in the large transverse momentum ($k_T \approx \mu$) limit as $\mu \rightarrow \infty$.

However, most implementations of TMD phenomenology from the past decade find tension between the extracted TMD functions and their large transverse momentum limits as calculated in fixed order collinear factorization. Consider, for instance, the far right panel in Fig. 6 of [10]. The pale blue dot-dashed curve is the cross section calculation performed with TMD pdfs and ffs (the so-called “ W term” or “TMD term”). This is to be compared with the dashed green curve (the “asymptotic” term), which represents the large transverse momentum asymptote of the cross section, calculated theoretically in collinear factorization. In principle, consistency demands that the TMD term and the asymptotic term approximately overlap in a range of $\Lambda_{\text{QCD}} \ll q_T \ll Q$. As the figure illustrates, this is not the case, at least for calculations done with standard parametrizations of collinear and TMD functions. It is only at the extremely high energies, shown in the far left plot, that a region starts to emerge where the asymptotic and TMD terms (very roughly) begin to overlap at intermediate transverse momentum. While the exact details of the mismatch depend on the specifics of the implementation, the trend appears to be quite general [11–14], and it applies to other processes where TMD factorization is often used¹. The overall picture suggests that elements are still missing from the standard way that TMD factorization gets implemented at a practical level.

A separate issue is that, for transverse momentum comparable to the hard scale ($q_T \approx Q$), the small $q_T \ll Q$ approximation fails and a so-called “ Y -term” is needed in order to get an accurate cross section calculation. However, the consistency problems alluded to above appear already at the level of the $q_T \ll Q$ contribution. In past papers, this small- q_T contribution has sometimes been called the “ W -term,” and it is the contribution that involves TMD correlation functions. It, and the TMD correlation functions from which it is composed, is the main focus of this paper. Throughout this paper, we will call it the “TMD term” to emphasize its connection to TMD pdfs and ffs.

In this paper, we will show how to recover consistency between the TMD term and the large- q_T asymptote by using an approach recently introduced by two of us [16]. In the process, we will diagnose some of the complications that, in the past, have been responsible for a mismatch. One problem arises from the way one imposes constraints of the form

$$f_{i/p}(x) \approx \int d^2\mathbf{k}_T f_{i/p}(x, \mathbf{k}_T), \quad (1)$$

where here there is an “ \approx ” rather than a strict equality because such integrals are generally ultraviolet (UV) divergent and are only satisfied literally in a strict parton model interpretation where the pdf is a literal probability density. To maintain a partonic interpretation, one hopes to preserve an approximate version of Eq. (1) as accurately as possible. For a given parametrization of $f_{i/p}(x)$, the parameters in a model of the nonperturbative transverse momentum in $f_{i/p}(x, \mathbf{k}_T)$ are constrained by Eq. (1). Now, in standard procedures for implementing the Collins-Soper-Sterman (CSS) formalism and similar approaches to TMD factorization, the nonperturbative transverse momentum dependence is contained within transverse coordinate space functions that are usually labeled $g_{i/p}(x, \mathbf{b}_T)$ (and $g_K(\mathbf{b}_T)$ for the Collins-Soper (CS) kernel). To our knowledge, however, constraints corresponding to Eq. (1) are never directly imposed upon the $g_{i/p}(x, \mathbf{b}_T)$ functions in phenomenological applications that use the g -function approach. As explained in Ref. [16], this will in general produce mismatches between the models of nonperturbative transverse momentum and the collinear functions $f_{i/p}(x)$ that are used to describe the perturbative tails. We will see with explicit examples in this paper that the effects of the mismatch can propagate in transverse momentum space and spoil the matching at intermediate regions of transverse momentum. Although we will mainly use standard $\overline{\text{MS}}$ collinear pdfs and ffs for the parts of calculations that require collinear factorization, we will sometimes find it convenient in intermediate steps to work with collinear pdfs and ffs defined as the transverse momentum integrals of TMD pdfs and ffs with UV cutoffs,

$$f^c(x; \mu) \equiv \pi \int_0^{\mu^2} dk_T^2 f_{i/p}(x, \mathbf{k}_T; \mu; \zeta), \quad (2)$$

where μ is the usual auxiliary mass parameter associated with $\overline{\text{MS}}$ renormalization and ζ is the CS scale. The “ c ” superscript on the left-hand side stands for “cutoff scheme.” As will be explained in the text, the cutoff-defined and $\overline{\text{MS}}$ pdfs and ffs can be translated into one another at large μ via relatively simple perturbative correction terms, so

¹ A successful implementation of the matching, that predates modern TMD factorization theorems, was presented in [15]

the choice of which one to use is ultimately largely a matter of convenience. However, the explicit expressions for Eq. (2) do have the advantage of a natural and direct connection to a TMD parton model interpretation.

A coherent treatment of the issues discussed above will be necessary in order for a meaningful analysis of future SIDIS data in terms of TMD parton correlation functions to be possible, and for the interpretability of, for example, forthcoming results from the CEBAF 12 GeV program or a 24 GeV upgrade [17], as well as for a future electron-ion collider (EIC). In Ref. [16] we called the treatment a “bottom-up” approach to distinguish it from more conventional treatments whose starting points were tailored to very high energies. In this paper we will instead call it the “hadron structure oriented” (HSO) approach to emphasize the central role of the nonperturbative input and the focus on preserving a partonic interpretation.

In this paper, we will set up the calculation of the TMD term for SIDIS using the HSO approach of [16], and we will analyze in detail the transition to the large q_T asymptotic term. We will show how imposing the integral relation in Eq. (2), ensuring a smooth transition between nonperturbative TMD behavior at small transverse momentum and the large transverse momentum tails, and several other adjustments to the conventional treatment fixes the problems outlined above. Specifically, we will show how to ensure that nonperturbative TMD pdf and ff parameterizations remain reasonably consistent with their expected large transverse momentum behavior, especially near the input scale. This work complements other efforts to address similar problems, for example [18, 19] imposes continuity and smoothness conditions on g -functions directly in coordinate space.

The structure of the paper is as follows: In Sec. II, we summarize the basic setup of SIDIS following the HSO organization of TMD factorization from [16]. We also explain the notation to be used throughout the paper. In Sec. III, we write down the general parametrizations of the TMD pdfs and ffs that we will use for calculations, and in Sec. IV we show how to specialize to specific models of the very small transverse momentum behavior, using Gaussian and spectator-motivated models for illustration. In Sec. V, we explain the calculation of the large transverse momentum asymptotic term in the HSO approach. In Sec. VI, we present sample calculations of the TMD term in SIDIS, with both the Gaussian and spectator inspired models for illustration. After analyzing how the conventional approach to TMD phenomenology leads to the complications discussed above, we show how they are solved in the HSO approach. We end in Sec. VII by discussing future plans for implementing phenomenological treatments in the HSO approach.

II. SEMI-INCLUSIVE DIS

We will adopt standard conventions for expressing SIDIS cross sections in the current fragmentation region, and our labels for the kinematical variables are mostly consistent with those of [20]. A lepton with momentum l scatters off a hadron target with momentum p , and the momentum of the recoiling lepton is l' . The final state contains a measured hadron with momentum P_B and is inclusive in all other final states X :

$$l + p \rightarrow l' + P_B + X \quad (3)$$

Throughout this paper, we will use the usual Lorentz invariant kinematical variables,

$$q^2 = -Q^2, \quad x_{bj} = \frac{Q^2}{2p \cdot q}, \quad z_h = \frac{P_B \cdot p}{p \cdot q}, \quad (4)$$

where $q \equiv (l - l')$ is the momentum of the exchanged photon. Except where specified, we will work in the Breit frame, with the proton moving in the plus light-cone direction (see figure 1). We will drop all power-suppressed target and final state kinematical mass corrections so that Breit frame momentum fractions are

$$x_N \equiv -\frac{p^+}{q^+} \approx x_{bj}, \quad (5)$$

where the “ \approx ” is a reminder that this identification only holds up to target power suppressed target mass corrections.

For characterizing regions of transverse momentum, we will use the variable

$$\mathbf{q}_T \equiv -\frac{\mathbf{P}_{BT}}{z_N}. \quad (6)$$

Here, \mathbf{q}_T is the transverse momentum of the virtual photon in a frame, which we call the “hadron frame,” where the target and final state hadrons are exactly back-to-back, and

$$z_N \equiv \frac{P_B^-}{q^-}. \quad (7)$$

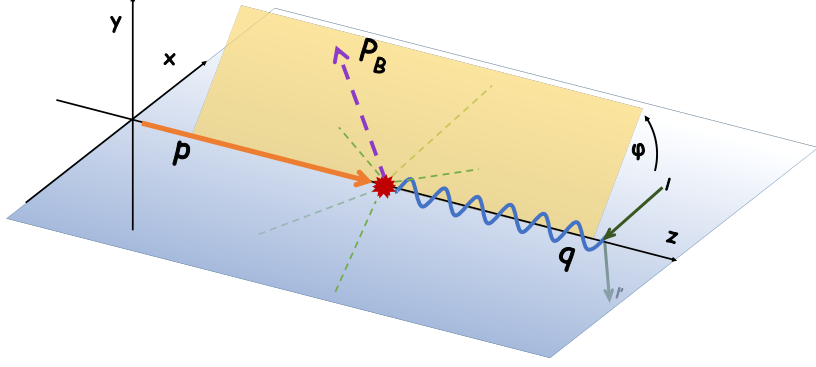


FIG. 1: Schematic of a SIDIS event as observed in the Breit frame. The dashed green lines represent the unobserved particles after the collision.

More details concerning the basic kinematical setup that we use may be found in [20]. In this paper, we will work in a strictly leading power approach, where $x_{bj} \approx x_N$ and $z_N \approx z_h$. To simplify notation, therefore, we will drop the subscripts on x and z from here forward.

Describing the cross section accurately over the full range of q_T requires that one merge the treatment tailored to the $q_T/Q \ll 1$ region (the TMD term) with the collinear factorization treatment appropriate to the $q_T \approx Q$ region. Both calculations must agree approximately in the intermediate $\Lambda_{QCD} \ll q_T \ll Q$ region. It is the treatment of the $q_T \ll Q$ region that involves TMD pdfs and ffs, and it is this contribution that we will focus on in this paper. In the small q_T limit, and neglecting kinematical hadron mass corrections, $z_N \approx z$.

The usual TMD-factorization expression for the hadronic tensor is

$$\begin{aligned}
W^{\mu\nu}(x, Q, z, \mathbf{P}_{BT}) &= \sum_j H_j^{\mu\nu} \int d^2\mathbf{k}_{1T} d^2\mathbf{k}_{2T} f_{j/p}(x, \mathbf{k}_{1T}; \mu_Q, Q^2) D_{h/j}(z, z\mathbf{k}_{2T}; \mu_Q, Q^2) \delta^{(2)}(\mathbf{q}_T + \mathbf{k}_{1T} - \mathbf{k}_{2T}) \\
&= \sum_j H_j^{\mu\nu} \int \frac{d^2\mathbf{b}_T}{(2\pi)^2} e^{-i\mathbf{q}_T \cdot \mathbf{b}_T} \tilde{f}_{j/p}(x, \mathbf{b}_T; \mu_Q, Q^2) \tilde{D}_{h/j}(z, \mathbf{b}_T; \mu_Q, Q^2) \\
&= \sum_j H_j^{\mu\nu} [f_{j/p}, D_{h/j}], \tag{8}
\end{aligned}$$

where the sum is over all quark and antiquark flavors, and each line is a different way that SIDIS routinely gets presented in the literature. The functions $f_{j/p}(x, \mathbf{k}_{1T}; \mu_Q, Q^2)$ and $D_{h/j}(z, z\mathbf{k}_{2T}; \mu_Q, Q^2)$ are the TMD pdfs and ffs respectively, with their usual operator definitions [3]. Within the approximations that define TMD factorization in the current region, the longitudinal momentum fractions of the incoming and struck partons are fixed to x and z . The momentum variables \mathbf{k}_{1T} and \mathbf{k}_{2T} are the transverse momenta of the struck and final state partons in the *hadron* frame, and we have fixed the auxiliary renormalization and light-cone scales μ and $\sqrt{\zeta}$ in Eq. (2) equal to μ_Q and Q respectively. (Ultimately, we will set $\mu_Q = Q$, but for organizational purposes we will keep the symbols separate for now.) $H_j^{\mu\nu}$ is a known hard coefficient. In transverse coordinate space, the TMD pdfs and ffs are

$$\begin{aligned}
\tilde{f}_{j/p}(x, \mathbf{b}_T; \mu, \zeta) &= \int d^2\mathbf{k}_{1T} e^{-i\mathbf{k}_{1T} \cdot \mathbf{b}_T} f_{j/p}(x, \mathbf{k}_{1T}; \mu, \zeta), \\
\tilde{D}_{q/j}(z, \mathbf{b}_T; \mu, \zeta) &= \int d^2\mathbf{k}_{2T} e^{i\mathbf{k}_{2T} \cdot \mathbf{b}_T} D_{q/j}(z, z\mathbf{k}_{2T}; \mu, \zeta), \tag{9}
\end{aligned}$$

and we have used these in the transverse coordinate space representation of $W^{\mu\nu}$ on the third line of Eq. (8), which is the standard form for implementing evolution. On the last line of Eq. (8), we have used the common bracket notation for abbreviating the transverse convolution integrals. The hard factor is

$$H_j^{\mu\nu} = \frac{z}{2} \text{Tr}[\gamma^\nu \gamma^+ \gamma^\mu \gamma^-] |H|_j^2 \tag{10}$$

where the last factor (see, for instance [21]) reads

$$|H_j^2 = e_j^2 \left\{ 1 + \frac{C_F \alpha_s(\mu)}{4\pi} \left[-16 + \frac{\pi^2}{3} + 6 \ln \left(\frac{Q^2}{\mu^2} \right) - 2 \ln^2 \left(\frac{Q^2}{\mu^2} \right) \right] + O(\alpha_s^2(\mu)) \right\}. \quad (11)$$

Projection tensors applied to Eq. (8) give the usual unpolarized quark structure functions of SIDIS,

$$F_{1,2}(x, Q, z, \mathbf{P}_{BT}) = P_{1,2}^{\mu\nu} W_{\mu\nu}(p, q, z, \mathbf{P}_{BT}), \quad (12)$$

where, still dropping kinematical hadron mass corrections,

$$P_1^{\mu\nu} = -\frac{1}{2} \left[g^{\mu\nu} - 4x^2 \frac{p^\mu p^\nu}{Q^2} \right], \quad (13a)$$

$$P_2^{\mu\nu} = -x \left[g^{\mu\nu} - 12x^2 \frac{p^\mu p^\nu}{Q^2} \right], \quad (13b)$$

and

$$\begin{aligned} P_1^{\mu\nu} H_{j,\mu\nu} &= H_1 = 2z |H_j^2|, \\ P_2^{\mu\nu} H_{j,\mu\nu} &= H_2 = 4zx |H_j^2|. \end{aligned} \quad (14)$$

Reference [16] substantially reorganized the more standard ways of expressing the TMD factorization expression for $W^{\mu\nu}$, as summarized by the sequence of steps in Sec. VI of that paper. Doing so required a high degree of specificity about exactly which versions of pdfs and ffs and their parametrizations were being discussed in a given context, and this led us to introduce a rather elaborate system of notation. For conciseness, we will drop most of that notation in this paper and instead indicate in the text which version of a symbol is being used whenever such distinctions become necessary. When we calculate Eq. (8), we will mostly be interested in using the final underlined $\tilde{f}_{j/p}$, $\tilde{D}_{h/j}$ in Eq. (61) of [16], although for the input scale calculations in this paper the difference between the underlined and “input” distributions is negligible. Any perturbatively calculable quantities will be maintained through order α_s , so results are all $O(\alpha_s)$. Any collinear pdfs or ffs should be assumed to be defined in the $\overline{\text{MS}}$ renormalization scheme unless otherwise specified. Power suppressed errors will be expressed as $O(m^2/Q^2)$ where m symbolizes any small mass scale like Λ_{QCD} or a hadron mass.

To implement evolution, we rewrite Eq. (8) in a form where each TMD function is expressed in terms of evolution from an input scale Q_0 . Thus, we use (the SIDIS version of) Eq. (65) from [16],

$$\begin{aligned} W^{\mu\nu}(x, Q, z, \mathbf{P}_{BT}) &= \sum_j H_j^{\mu\nu} \int \frac{d^2 \mathbf{b}_T}{(2\pi)^2} e^{-i\mathbf{q}_T \cdot \mathbf{b}_T} \tilde{f}_{j/p}(x, \mathbf{b}_T; \mu_{Q_0}, Q_0^2) \tilde{D}_{h/j}(z, \mathbf{b}_T; \mu_{Q_0}, Q_0^2) \\ &\times \exp \left\{ \tilde{K}(b_T; \mu_{Q_0}) \ln \left(\frac{Q^2}{Q_0^2} \right) + \int_{\mu_{Q_0}}^{\mu} \frac{d\mu'}{\mu'} \left[2\gamma(\alpha_s(\mu'); 1) - \ln \frac{Q^2}{\mu'^2} \gamma_K(\alpha_s(\mu')) \right] \right\}. \end{aligned} \quad (15)$$

Q_0 should be understood to be the lowest value of Q for which factorization techniques are considered reasonable, which in practice is usually between around 1 GeV and 4 GeV for SIDIS. An important observation underlying the HSO approach of Ref. [16] is that individual correlation functions, $f_{j/p}(x, \mathbf{k}_T; \mu_{Q_0}, Q_0^2)$ or $\tilde{D}_{h/j}(z, \mathbf{b}_T; \mu_{Q_0}, Q_0^2)$, have unambiguous transverse momentum dependence for all k_T , including all $k_T > Q_0$, which follows from their operator definitions. Once these input functions have been determined, evolving them to larger Q is only a matter of substituting them into Eq. (15) (after transforming into coordinate space). This can be used to simplify the organization of phenomenological implementations because one may focus attention on the nonperturbative momentum space treatment of hadron structure at Q near the initial input scale Q_0 . The only input that is then necessary to obtain the TMDs at any other higher scale is the evolution kernel.

In this paper, we will be mostly interested in the behavior of the input TMD pdfs and ffs, in which case the evolution factor does not enter. In places where we do need the evolution factor, we will use the same parametrization for the CS kernel from Sec. VII-A from Ref. [16] since it reproduces the correct $O(\alpha_s)$ perturbative behavior while also capturing minimal basic expectations for the nonperturbative behavior. Thus, the input scale parametrization of the kernel that we will use is

$$\tilde{K}_{\text{inpt}}(b_T; \mu_{Q_0}) = \frac{2\alpha_s(\mu_{Q_0})C_F}{\pi} \left[K_0(b_T m_K) + \ln \left(\frac{m_K}{\mu_{Q_0}} \right) \right] \quad (16)$$

so the full (underlined, in the notation of Ref. [16]) kernel is

$$\tilde{K}(b_T; \mu_{Q_0}) = \frac{2\alpha_s(\mu_{\bar{Q}_0})C_F}{\pi} \left[K_0(b_T m_K) + \ln \left(\frac{m_K}{\mu_{\bar{Q}_0}} \right) \right] - \int_{\mu_{\bar{Q}_0}}^{\mu_{Q_0}} \frac{d\mu'}{\mu'} \gamma_K(\alpha_s(\mu')). \quad (17)$$

The nonperturbative model parameter in $\tilde{K}(b_T; \mu_{Q_0})$ is m_K . The bar on top of \bar{Q}_0 and $\mu_{\bar{Q}_0}$ is the symbol introduced in [16] to indicate that this is a scale that is fixed to Q_0 at large b_T , but which transitions to $\sim 1/b_T$ behavior as $b_T \rightarrow 0$. The role of the ‘‘scale transformation function’’, \bar{Q}_0 , is analogous to that of b_* in the usual CSS treatment, and its exact choice is, in principle, arbitrary. We will continue to use the choice for \bar{Q}_0 from Ref. [16]. We provide the expression in Appendix A of this paper. We remark that it is possible to consider other types of nonperturbative behavior for the CS kernel within the approach of Ref. [16], including recent calculations in lattice QCD (see for instance Refs. [22–25]).

III. TMD PARTON DENSITY & FRAGMENTATION FUNCTIONS

For constructing parametrizations of the quark and antiquark TMD pdfs and ffs, we repeat the steps in Sec.VI of Ref. [16]. We continue to use the additive structure from the examples in Ref. [16] to interpolate between a nonperturbative core and the perturbative tail. The first terms transition into the fixed $O(\alpha_s(\mu))$ tail calculation of the TMD at large k_T , while the last term is a non-perturbative ‘‘core’’ that describes the peak at very small k_T . The core term is further constrained by an integral relation analogous to Eq. (2), which determines its overall normalization factor $C_{h/j}$.

Thus, for the input quark ff

$$\begin{aligned} D_{\text{inpt},h/j}(z, z\mathbf{k}_T; \mu_{Q_0}, Q_0^2) &= \frac{1}{2\pi z^2} \frac{1}{k_T^2 + m_{D_{h,j}}^2} \left[A_{h/j}^D(z; \mu_{Q_0}) + B_{h/j}^D(z; \mu_{Q_0}) \ln \frac{Q_0^2}{k_T^2 + m_{D_{h,j}}^2} \right] \\ &+ \frac{1}{2\pi z^2} \frac{1}{k_T^2 + m_{D_{h,g}}^2} A_{h/j}^{D,g}(z; \mu_{Q_0}) \\ &+ C_{h/j}^D D_{\text{core},h/j}(z, z\mathbf{k}_T; Q_0^2), \end{aligned} \quad (18)$$

where $D_{\text{core},h/j}(z, z\mathbf{k}_T; Q_0^2)$ is a parametrization of the peak of the TMD ff to be specified later. To compactify notation, we have dropped the (n, d_r) superscripts that were used in [16], but we have included a hadron label h and $j \in u, d, s, c, \dots$ labels for parton flavors and anti-flavors. A^D , B^D , and C^D are abbreviations for the following expressions,

$$A_{h/j}^D(z; \mu_{Q_0}) \equiv \sum_{jj'} \delta_{j'j} \frac{\alpha_s(\mu_{Q_0})}{\pi} \left\{ [(P_{jj'} \otimes d_{h/j'})(z; \mu_{Q_0})] - \frac{3C_F}{2} d_{h/j'}(z; \mu_{Q_0}) \right\}, \quad (19)$$

$$B_{h/j}^D(z; \mu_{Q_0}) \equiv \sum_{jj'} \delta_{j'j} \frac{\alpha_s(\mu_{Q_0})C_F}{\pi} d_{h/j'}(z; \mu_{Q_0}), \quad (20)$$

$$A_{h/j}^{D,g}(z; \mu_{Q_0}) \equiv \frac{\alpha_s(\mu_{Q_0})}{\pi} [(P_{gj} \otimes d_{h/g})(z; \mu_{Q_0})], \quad (21)$$

$$\begin{aligned} C_{h/j}^D &\equiv \frac{1}{N_{h/j}^D} \left[d_{h/j}(z; \mu_{Q_0}) - A_{h/j}^D(z; \mu_{Q_0}) \ln \left(\frac{\mu_{Q_0}}{m_{D_{h,j}}} \right) - B_{h/j}^D(z; \mu_{Q_0}) \ln \left(\frac{\mu_{Q_0}}{m_{D_{h,j}}} \right) \ln \left(\frac{Q_0^2}{\mu_{Q_0} m_{D_{h,j}}} \right), \right. \\ &\left. - A_{h/j}^{D,g}(z; \mu_{Q_0}) \ln \left(\frac{\mu_{Q_0}}{m_{D_{h,g}}} \right) + \frac{\alpha_s(\mu_{Q_0})}{2\pi} \left\{ \sum_{jj'} \delta_{j'j} [C_{\Delta}^{j'/j} \otimes d_{h/j'}](z; \mu_{Q_0}) + [C_{\Delta}^{g/j} \otimes d_{h/g}](z; \mu_{Q_0}) \right\} \right]. \end{aligned} \quad (22)$$

where

$$P_{qq}(z) = P_{\bar{q}\bar{q}}(z) = C_F \left[\frac{1+z^2}{(1-z)_+} + \frac{3}{2} \delta(1-z) \right], \quad (23)$$

$$P_{gq}(z) = C_F \frac{1+(1-z)^2}{z}, \quad (24)$$

$$\mathcal{C}_\Delta^{q/q}(z) = 2P_{qq}(z) \ln z + C_F(1-z) - C_F \frac{\pi^2}{12} \delta(1-z), \quad (25)$$

$$\mathcal{C}_\Delta^{g/q}(z) = 2P_{gq}(z) \ln z + C_F z, \quad (26)$$

$$N_{h/j}^D \equiv 2\pi z^2 \int_0^\infty dk_T k_T D_{\text{core},h/j}(z, z\mathbf{k}_T; Q_0^2). \quad (27)$$

For the TMD pdfs, the expressions are similar,

$$\begin{aligned} f_{\text{inpt},i/p}(x, \mathbf{k}_T; \mu_{Q_0}, Q_0^2) &= \frac{1}{2\pi} \frac{1}{k_T^2 + m_{f_{i,p}}^2} \left[A_{i/p}^f(x; \mu_{Q_0}) + B_{i/p}^f(x; \mu_{Q_0}) \ln \frac{Q_0^2}{k_T^2 + m_{f_{i,p}}^2} \right] \\ &+ \frac{1}{2\pi} \frac{1}{k_T^2 + m_{f_{g,p}}^2} A_{i/p}^{f,g}(x; \mu_{Q_0}) \\ &+ C_{i/p}^f f_{\text{core},i/p}(x, \mathbf{k}_T; Q_0^2), \end{aligned} \quad (28)$$

with the corresponding abbreviations

$$A_{i/p}^f(x; \mu_{Q_0}) \equiv \sum_{ii'} \delta_{i'i} \frac{\alpha_s(\mu_{Q_0})}{\pi} \left\{ [(P_{i'i} \otimes f_{i'/p})(x; \mu_{Q_0})] - \frac{3C_F}{2} f_{i'/p}(x; \mu_{Q_0}) \right\}, \quad (29)$$

$$B_{i/p}^f(x; \mu_{Q_0}) \equiv \sum_{i'i} \delta_{i'i} \frac{\alpha_s(\mu_{Q_0}) C_F}{\pi} f_{i'/p}(x; \mu_{Q_0}), \quad (30)$$

$$A_{i/p}^{f,g}(x; \mu_{Q_0}) \equiv \frac{\alpha_s(\mu_{Q_0})}{\pi} [(P_{ig} \otimes f_{g/p})(x; \mu_{Q_0})], \quad (31)$$

$$\begin{aligned} C_{i/p}^f &\equiv \frac{1}{N_{i/p}^f} \left[f_{i/p}(x; \mu_{Q_0}) - A_{i/p}^f(x; \mu_{Q_0}) \ln \left(\frac{\mu_{Q_0}}{m_{f_{i,p}}} \right) - B_{i/p}^f(x; \mu_{Q_0}) \ln \left(\frac{\mu_{Q_0}}{m_{f_{i,p}}} \right) \ln \left(\frac{Q_0^2}{\mu_{Q_0} m_{f_{i,p}}} \right) \right. \\ &\left. - A_{i/p}^{f,g}(x; \mu_{Q_0}) \ln \left(\frac{\mu_{Q_0}}{m_{f_{g,p}}} \right) + \frac{\alpha_s(\mu_{Q_0})}{2\pi} \left\{ \sum_{ii'} \delta_{i'i} [\mathcal{C}_\Delta^{i/i'} \otimes f_{i'/p}](x; \mu_{Q_0}) + [\mathcal{C}_\Delta^{i/g} \otimes f_{g/p}](x; \mu_{Q_0}) \right\} \right]. \end{aligned} \quad (32)$$

where

$$P_{ig}(x) = T_F [x^2 + (1-x)^2], \quad (33)$$

$$\mathcal{C}_\Delta^{i/i}(x) = C_F(1-x) - C_F \frac{\pi^2}{12} \delta(1-x), \quad (34)$$

$$\mathcal{C}_\Delta^{g/p}(x) = 2T_F x(1-x), \quad (35)$$

$$N_{i/p}^f \equiv 2\pi \int_0^\infty dk_T k_T f_{\text{core},i/p}(x, \mathbf{k}_T; Q_0^2) \quad (36)$$

In Eq. (28), $f_{\text{core},i/p}(x, \mathbf{k}_T; Q_0^2)$ parametrizes the core peak of the TMD pdf. (We remind the reader that it is to be understood that all explicit perturbative parts in this paper are calculated to lowest order in α_s .)

To extend the TMD pdf and ff parametrizations above to account for the $b_T \ll 1/Q_0$ region, we transform to transverse coordinate space and use Eq. (92) of [16] and its analog for the TMD pdf,

$$\tilde{D}_{h/j}(z, \mathbf{b}_T; \mu_{Q_0}, Q_0^2) = \tilde{D}_{\text{inpt},h/j}(z, \mathbf{b}_T; \mu_{\bar{Q}_0}, \bar{Q}_0^2) E(\bar{Q}_0/Q_0, b_T). \quad (37)$$

$$\tilde{f}_{i/p}(x, \mathbf{b}_T; \mu_{Q_0}, Q_0^2) = \tilde{f}_{\text{inpt},i/p}(x, \mathbf{b}_T; \mu_{\bar{Q}_0}, \bar{Q}_0^2) E(\bar{Q}_0/Q_0, b_T). \quad (38)$$

with an evolution factor

$$E(\bar{Q}_0/Q_0, b_T) \equiv \exp \left\{ \int_{\mu_{\bar{Q}_0}}^{\mu_{Q_0}} \frac{d\mu'}{\mu'} \left[\gamma(\alpha_s(\mu'); 1) - \ln \frac{Q_0}{\mu'} \gamma_K(\alpha_s(\mu')) \right] + \ln \frac{Q_0}{\bar{Q}_0} \tilde{K}_{\text{inpt}}(b_T; \mu_{\bar{Q}_0}) \right\}. \quad (39)$$

Once the numerical values of parameters in $\tilde{D}_{h/j}(z, \mathbf{b}_T; \mu_{Q_0}, Q_0^2)$ and $\tilde{f}_{i/p}(x, \mathbf{b}_T; \mu_{Q_0}, Q_0^2)$ are determined and fixed as above, the TMD term at any other larger scale Q is found straightforwardly by substituting these into Eq. (15).

The scale \bar{Q}_0 is designed to be approximately Q_0 for $Q \approx Q_0$, where the only important range of b_T is $b_T \gtrsim 1/Q_0$, and the left and right sides of Eqs. (37)–(38) are nearly equal. For large Q ($Q \gg Q_0$), the UV $b_T \ll 1/Q_0$ region starts to become important and cannot be ignored. There, \bar{Q}_0 smoothly transitions into a $\sim 1/b_T$ behavior such that RG improvement is implemented in the $\mathbf{b}_T \rightarrow \mathbf{0}_T$ limit. The left sides of Eqs. (37)–(38) are the parametrizations that we labeled with underlines in Eq.(60) of Ref. [16], while the “input” functions on the left sides are to be used for phenomenological fitting for $Q \approx Q_0$. By construction, the left and right sides of Eqs. (37)–(38), as well Q_0 and \bar{Q}_0 , differ negligibly in the range of b_T relevant to $Q \approx Q_0$ phenomenology – recall the discussion in Sec. V of [16].

For the examples implementations we will perform in Sec. VID, we will use the approximation

$$E(\bar{Q}_0/Q_0, b_T) \approx 1, \quad (40)$$

and set $\bar{Q}_0 \rightarrow Q_0$, since for this paper our main focus is on the $Q \approx Q_0$ region and the construction of satisfactory parametrizations for $\tilde{D}_{\text{inpt},h/j}(z, \mathbf{b}_T; \mu_{Q_0}, Q_0^2)$ and $\tilde{f}_{\text{inpt},i/p}(x, \mathbf{b}_T; \mu_{Q_0}, Q_0^2)$. At the end of Sec. VID, we will restore the \bar{Q}_0 treatment and confirm that its effect is negligible at $Q \approx Q_0$.

It can be seen by inspection that the input parametrizations defined in Eq. (18) and Eq. (28) are constrained to match the perturbative large- k_T collinear factorization approximations for the TMD pdfs and ffs,

$$D_{\text{inpt},h/j}^{\text{pert}}(z, z\mathbf{k}_T; \mu_{Q_0}, Q_0^2) = \frac{1}{2\pi z^2} \frac{1}{k_T^2} \left[A_{h/j}^D(z; \mu_{Q_0}) + B_{h/j}^D(z; \mu_{Q_0}) \ln \frac{Q_0^2}{k_T^2} \right] + \frac{1}{2\pi z^2} \frac{1}{k_T^2} A_{h/j}^{D,g}(z; \mu_{Q_0}), \quad (41)$$

$$f_{\text{inpt},i/p}^{\text{pert}}(x, \mathbf{k}_T; \mu_{Q_0}, Q_0^2) = \frac{1}{2\pi} \frac{1}{k_T^2} \left[A_{i/p}^f(x; \mu_{Q_0}) + B_{i/p}^f(x; \mu_{Q_0}) \ln \frac{Q_0^2}{k_T^2} \right] + \frac{1}{2\pi} \frac{1}{k_T^2} A_{i/p}^{f,g}(x; \mu_{Q_0}), \quad (42)$$

which are good approximations to the true TMD correlation functions when $k_T \approx Q_0$ and $Q_0 \gg m$. Equations (41) and (42) are calculable entirely within leading power collinear factorization. The same expressions apply at any value of Q , but for this paper we are especially interested in Q near the input scale.

IV. GAUSSIAN VERSUS SCALAR DIQUARK MODELS

The model parametrizations of the last section are still quite general. The only choices that have been made so far are to use an additive structure to interpolate to the order- α_s perturbative tail at $k_T \approx Q_0$ and the choice of the parametrization of the CS kernel in Eq. (17). Further assumptions are necessary before these parametrizations can become useful.

Most of the effort in nonperturbative modeling enters in the choices for the functional forms for $D_{\text{core},h/j}(z, z\mathbf{k}_T; Q_0^2)$ and $f_{\text{core},i/p}(x, \mathbf{k}_T; Q_0^2)$ that describe the very small $k_T \approx 0_T$ behavior. However, many approaches to modeling or parametrizing this region of nonperturbative TMDs already exist [26–47], and one may defer to them at this stage in the parametrization construction. The only way these previously existing models need to be modified is by including the interpolation to the order α_s large- k_T behavior, and by imposing integral relations analogous to Eq. (2). All that remains is to adjust $D_{\text{core},h/j}(z, z\mathbf{k}_T; Q_0^2)$ and $f_{\text{core},i/p}(x, \mathbf{k}_T; Q_0^2)$ so as to recover (at least approximately) existing model parametrizations in the $k_T \approx 0$ region. The parameters $m_{D_{j,h}}, m_{D_{g,h}}, m_{f_{i,p}}, m_{f_{g,p}}$ control the transition between the k_T model and the large k_T perturbative tail.

For the purposes of this article, we will focus on two of the most commonly used models in phenomenology that are simple to implement. The first is the Gaussian model of TMDs (see, for example, Refs.[48–50]), which is often found to successfully describe data at lower Q . It prescribes the functions forms

$$f_{\text{core},i/p}^{\text{Gauss}}(x, \mathbf{k}_T; Q_0^2) = \frac{e^{-k_T^2/M_F^2}}{\pi M_F^2}, \quad D_{\text{core},h/j}^{\text{Gauss}}(z, z\mathbf{k}_T; Q_0^2) = \frac{e^{-z^2 k_T^2/M_D^2}}{\pi M_D^2}. \quad (43)$$

The second model that we will consider is inspired by the popular spectator diquark model [28, 51]. For it, we adopt

the functional forms

$$f_{\text{core},i/p}^{\text{Spect}}(x, \mathbf{k}_T; Q_0^2) = \frac{6M_{0F}^6}{\pi(2M_F^2 + M_{0F}^2)} \frac{M_F^2 + k_T^2}{(M_{0F}^2 + k_T^2)^4}. \quad (44)$$

$$D_{\text{core},h/j}^{\text{Spect}}(z, z\mathbf{k}_T; Q_0^2) = \frac{2M_{0D}^4}{\pi(M_D^2 + M_{0D}^2)} \frac{M_D^2 + k_T^2 z^2}{(M_{0D}^2 + k_T^2 z^2)^3}, \quad (45)$$

The overall factors in Eqs. (43)–(45) are chosen so that $N_{h/j}^D = N_{i/p}^f = 1$ in both models (recall Eq. (27) and Eq. (36)).

In later sections, it will often be convenient to work with collinear pdfs and ffs defined as the cutoff transverse momentum integrals of TMD pdfs and ffs. Hence, we define

$$f_{i/p}^c(x; \mu_Q) \equiv 2\pi \int_0^{\mu_Q} dk_T k_T f_{i/p}(x, \mathbf{k}_T; \mu_Q, Q^2), \quad (46)$$

$$d_{h/j}^c(z; \mu_Q) \equiv 2\pi z^2 \int_0^{\mu_Q} dk_T k_T D_{h/j}(z, z\mathbf{k}_T; \mu_Q, Q^2), \quad (47)$$

where the c superscript stands for ‘‘cutoff.’’ The cutoff definitions could be defined more generally with an upper limit μ_f different from μ_Q , but we will keep these scales equal for the present paper. The cutoff and $\overline{\text{MS}}$ -renormalized definitions are equal up to a scheme change and m^2/μ_Q^2 -suppressed corrections.

With our parametrizations of TMD pdfs and ffs in the previous section, the integrals are

$$\begin{aligned} f_{\text{inpt},i/p}^c(x; \mu_{Q_0}) &= 2\pi \int_0^{\mu_{Q_0}} dk_T k_T f_{\text{inpt},i/p}(x, \mathbf{k}_T; \mu_{Q_0}, Q_0^2) = \\ & C_{i/p}^f f_{\text{core},i/p}^c(x; \mu_{Q_0}) + \frac{1}{2} A_{i/p}^{f,g}(x; \mu_{Q_0}) \ln \left(1 + \frac{\mu_{Q_0}^2}{m_{f,g,p}^2} \right) \\ & + \frac{1}{2} A_{i/p}^f(x; \mu_{Q_0}) \ln \left(1 + \frac{\mu_{Q_0}^2}{m_{f,i,p}^2} \right) + \frac{1}{4} B_{i/p}^f(x; \mu_{Q_0}) \left[\ln^2 \left(\frac{m_{f,i,p}^2}{Q_0^2} \right) - \ln^2 \left(\frac{\mu_{Q_0}^2 + m_{f,i,p}^2}{Q_0^2} \right) \right] \\ & = f_{i/p}(x; \mu_{Q_0}) + O \left(\alpha_s(\mu_0)^2, \frac{m^2}{Q_0^2} \right), \end{aligned} \quad (48)$$

and

$$\begin{aligned} d_{\text{inpt},h/j}^c(z; \mu_{Q_0}) &= 2\pi z^2 \int_0^{\mu_{Q_0}} dk_T k_T D_{\text{inpt},h/j}(z, z\mathbf{k}_T; \mu_{Q_0}, Q_0^2) = \\ & C_{h/j}^D d_{\text{core},h/j}^c(z; \mu_{Q_0}) + \frac{1}{2} A_{h/j}^{D,g}(z; \mu_{Q_0}) \ln \left(1 + \frac{\mu_{Q_0}^2}{m_{D,h,g}^2} \right) \\ & + \frac{1}{2} A_{h/j}^D(z; \mu_{Q_0}) \ln \left(1 + \frac{\mu_{Q_0}^2}{m_{D,h,j}^2} \right) + \frac{1}{4} B_{h/j}^D(z; \mu_{Q_0}) \left[\ln^2 \left(\frac{m_{D,h,j}^2}{Q_0^2} \right) - \ln^2 \left(\frac{\mu_{Q_0}^2 + m_{D,h,j}^2}{Q_0^2} \right) \right] \\ & = d_{h/j}(z; \mu_{Q_0}) + O \left(\alpha_s(\mu_0)^2, \frac{m^2}{Q_0^2} \right), \end{aligned} \quad (49)$$

with

$$f_{\text{core},i/p}^{c,\text{Gauss}}(x; \mu_{Q_0}, Q_0^2) = 1 - e^{-\mu_{Q_0}^2/M_F^2}, \quad d_{\text{core},h/j}^{c,\text{Gauss}}(z; \mu_{Q_0}, Q_0^2) = 1 - e^{-z^2 \mu_{Q_0}^2/M_D^2}, \quad (50)$$

in the case of the Gaussian model, and

$$f_{\text{core},i/p}^{c,\text{Spect}}(x; \mu_{Q_0}, Q_0^2) = 1 - \frac{M_{0F}^6 (2M_F^2 + M_{0F}^2 + 3\mu_{Q_0}^2)}{(2M_F^2 + M_{0F}^2) (M_{0F}^2 + \mu_{Q_0}^2)^3}, \quad (51)$$

$$d_{\text{core},h/j}^{c,\text{Spect}}(z; \mu_{Q_0}, Q_0^2) = 1 - \frac{M_{0D}^4 (M_D^2 + M_{0D}^2 + 2\mu_{Q_0}^2 z^2)}{(M_D^2 + M_{0D}^2) (M_{0D}^2 + \mu_{Q_0}^2 z^2)^2}. \quad (52)$$

in the case of the spectator model. Note that Eqs. (50)–(52) are all 1 up to (at most) $m^2/\mu_{Q_0}^2$ -suppressed errors.

The expressions in Eqs. (48)–(49) follow directly by substituting Eq. (18) and Eq. (28) into Eqs. (46)–(47). By substituting the expressions in Eq. (22) and Eq. (32) for $C_{h/j}^D$ and $C_{i/p}^f$, it is straightforward to verify that the collinear pdfs and ffs of Eq. (48) and Eq. (49) are equal to the standard $\overline{\text{MS}}$ $f(x; \mu_{Q_0})$ and $d(z; \mu_{Q_0})$ respectively in the limit that $O(m^2/Q_0^2)$ and $O(\alpha_s(\mu_{Q_0})^2)$ errors are negligible.

To further simplify later numerical examples and reduce the number of free parameters, in the spectator-like models we will fix $M_{0F} = M_{0D}/z = 0.2 \text{ GeV}$. We will also assume that model masses have no parton flavor dependence, and that the $M_{F,D}$ of the core distributions is the same as the $m_{f,D}$ in the tail terms. That is, for both models we will assume for now

$$m_{f_i,p} = m_{f_g,p} = M_F, \quad (53)$$

$$m_{D_{h,j}} = m_{D_{h,g}} = M_D. \quad (54)$$

In general, the parameters in Eqs. (53)–(54) could have different numerical values in the Gaussian and the spectator-like models, but we will keep the same labels in both to simplify notation.

It should be emphasized that nothing in the setup of Sec. III relies on the use of any *particular* nonperturbative model. Indeed, one of the motivating advantages of the HSO approach is that the momentum space nonperturbative model of the $k_T \approx 0$ region becomes easily interchangeable, as demonstrated by our switching between the Gaussian and spectator diquark models above.

V. THE LARGE TRANSVERSE MOMENTUM ASYMPTOTE

In this section, we will enumerate the steps for extracting the large- q_T asymptote of Eq. (15). These steps will be particularly relevant to phenomenological treatments of the $Q \approx Q_0$ region. Our path here differs from that of more standard presentations in that we start with the *small* transverse momentum part of the TMD term and extract the large $q_T \approx Q$ behavior, in contrast to the more usual steps that start with large- q_T calculations of the cross section in collinear perturbation theory and extract the $q_T \rightarrow 0$ asymptote. Both approaches must give the same result up to $O(m^2/Q^2)$ and $O(\alpha_s(Q)^{n+1})$ corrections.

In all steps below, we will assume we are analyzing the TMD term in a regime where q_T is comparable to Q and Q approaches infinity. To be specific, we take $q_T = \eta Q$ where η is a fixed, order unity constant and we let $m^2/Q^2 \rightarrow 0$. It will be convenient to first express the transverse momentum convolution integral on the second line of Eq. (8) in the following way,

$$[f, D] = \int d^2\mathbf{k}_T f(x, \mathbf{k}_T - \mathbf{q}_T/2; \mu_Q; Q^2) D(z, z(\mathbf{k}_T + \mathbf{q}_T/2); \mu_Q; Q^2), \quad (55)$$

where flavor subscripts are dropped. If we first consider the region of the integrand where

$$\mathbf{k}_T = \mathbf{q}_T/2 + O(m), \quad (56)$$

then

$$\begin{aligned} & f(x, \mathbf{k}_T - \mathbf{q}_T/2; \mu_Q; Q^2) D(z, z(\mathbf{k}_T + \mathbf{q}_T/2); \mu_Q; Q^2) \\ &= f(x, \mathbf{k}_T - \mathbf{q}_T/2; \mu_Q; Q^2) D^{\text{pert}}(z, z\mathbf{q}_T; \mu_Q; Q^2) + O\left(\frac{m^2}{q_T^2}\right). \end{aligned} \quad (57)$$

If we specialize to the order- α_s case, then the collinear perturbative expression from Eq. (41), appropriate to the $k_T \approx Q$ region, may be used for $D^{\text{pert}}(z, z\mathbf{q}_T; \mu_Q; Q^2)$. At order- α_s^n , higher order versions may be used. Likewise, if we consider the region where

$$\mathbf{k}_T = -\mathbf{q}_T/2 + O(m), \quad (58)$$

then

$$\begin{aligned} & f(x, \mathbf{k}_T - \mathbf{q}_T/2; \mu_Q; Q^2) D(z, z(\mathbf{k}_T + \mathbf{q}_T/2); \mu_Q; Q^2) \\ &= f^{\text{pert}}(x, -\mathbf{q}_T; \mu_Q; Q^2) D(z, z(\mathbf{k}_T + \mathbf{q}_T/2); \mu_Q; Q^2) + O\left(\frac{m^2}{q_T^2}\right), \end{aligned} \quad (59)$$

where $f^{\text{pert}}(x, -\mathbf{q}_T; \mu_Q; Q^2)$ is the n^{th} -order perturbative expression appropriate to $k_T \approx Q$. Again, when we specialize to the order- α_s treatment, the perturbative expression in Eq. (42) can be used, and at order- α_s^n , the higher order versions of these expressions may be used.

Having the expansions in Eq. (57) and Eq. (59) on hand motivates us to rewrite Eq. (55) in the form

$$\begin{aligned}
[f, D] &= D(z, z\mathbf{q}_T; \mu_Q; Q^2) \left(2\pi \int_0^{\mu_Q} dk_T k_T f(x, \mathbf{k}_T; \mu_Q; Q^2) \right) \\
&+ f(x, -\mathbf{q}_T; \mu_Q; Q^2) \left(2\pi \int_0^{\mu_Q} dk_T k_T D(z, z\mathbf{k}_T; \mu_Q; Q^2) \right) \\
&+ \int d^2\mathbf{k}_T \left\{ f(x, \mathbf{k}_T - \mathbf{q}_T/2; \mu_Q; Q^2) D(z, z(\mathbf{k}_T + \mathbf{q}_T/2); \mu_Q; Q^2) \right. \\
&\quad \left. - D(z, z\mathbf{q}_T; \mu_Q; Q^2) f(x, \mathbf{k}_T - \mathbf{q}_T/2; \mu_Q; Q^2) \Theta(\mu_Q - |\mathbf{k}_T - \mathbf{q}_T/2|) \right. \\
&\quad \left. - D(z, z(\mathbf{k}_T + \mathbf{q}_T/2); \mu_Q; Q^2) f(x, -\mathbf{q}_T; \mu_Q; Q^2) \Theta(\mu_Q - |\mathbf{k}_T + \mathbf{q}_T/2|) \right\}, \tag{60}
\end{aligned}$$

where we have simply added and subtracted the first two lines from the exact Eq. (55) to get the integral on the last three lines. On the first two lines of Eq. (60), we may replace $f(x, \mathbf{q}_T; \mu_Q; Q^2)$ and $D(z, z\mathbf{q}_T; \mu_Q; Q^2)$ by their perturbative collinear approximations from Eq. (57) and Eq. (59). Since they are evaluated at $\mathbf{q}_T \approx Q$, this only introduces power-suppressed errors. We may also identify the cutoff integrals on the first two lines with the cutoff definitions of the collinear pdfs and ffs in Eqs. (46)–(47). The integrand of the last three lines is suppressed by $O(m^2/q_T^2)$ in regions where $\mathbf{k}_T = \pm\mathbf{q}_T/2 + O(m)$. Therefore, we may restrict our consideration of its behavior to regions where

$$|\mathbf{k}_{1T}| = |\mathbf{k}_T - \mathbf{q}_T/2| \sim q_T, \tag{61}$$

$$|\mathbf{k}_{2T}| = |\mathbf{k}_T + \mathbf{q}_T/2| \sim q_T, \tag{62}$$

i.e., where both k_{1T} and k_{2T} are an order unity fraction of q_T . Then, all TMD pdfs and ffs in the integrand of the last three lines of Eq. (60) can be expanded in powers of m^2/q_T^2 and replaced by their perturbative approximations, with only power suppressed corrections. We thus have

$$\begin{aligned}
[f, D] &= D^{\text{pert}}(z, z\mathbf{q}_T; \mu_Q; Q^2) f^c(x; \mu_Q) + \frac{1}{z^2} f^{\text{pert}}(x, -\mathbf{q}_T; \mu_Q; Q^2) d^c(z; \mu_Q) \\
&+ \int d^2\mathbf{k}_T \left\{ f^{\text{pert}}(x, \mathbf{k}_T - \mathbf{q}_T/2; \mu_Q; Q^2) D^{\text{pert}}(z, z(\mathbf{k}_T + \mathbf{q}_T/2); \mu_Q; Q^2) \right. \\
&\quad \left. - D^{\text{pert}}(z, z\mathbf{q}_T; \mu_Q; Q^2) f^{\text{pert}}(x, \mathbf{k}_T - \mathbf{q}_T/2; \mu_Q; Q^2) \Theta(\mu_Q - |\mathbf{k}_T - \mathbf{q}_T/2|) \right. \\
&\quad \left. - D^{\text{pert}}(z, z(\mathbf{k}_T + \mathbf{q}_T/2); \mu_Q; Q^2) f^{\text{pert}}(x, -\mathbf{q}_T; \mu_Q; Q^2) \Theta(\mu_Q - |\mathbf{k}_T + \mathbf{q}_T/2|) \right\} + O\left(\frac{m^2}{q_T^2}\right) \\
&= [f, D]_{\text{ASY}} + O\left(\frac{m^2}{q_T^2}\right) \tag{63}
\end{aligned}$$

Dropping the $O(m^2/q_T^2)$ errors gives the asymptotic term that we sought. We will denote this ‘‘asymptotic’’ approximation by $[f, D]_{\text{ASY}}$, as indicated on the last line. It is calculable entirely within collinear perturbation theory, and it is an increasingly accurate approximate of the full cross section as $q_T \propto Q$ and $Q \rightarrow \infty$. The derivation above of Eq. (63) applies at any order of α_s , although for this paper we will be mostly interested in $O(\alpha_s)$ expressions.

Notice that it is the *cutoff* definitions, Eqs. (46)–(47), for the collinear functions, and not the usual $\overline{\text{MS}}$ definitions, that appear on the first line of Eq. (63). One recovers the full asymptotic term for the cross section by substituting this into Eq. (8).

To specialize to the $O(\alpha_s)$ case at an input scale $Q = Q_0$, with the parametrizations in Eqs. (18)–(28), one substitutes the expressions from Eqs. (41)–(42). Equations (48) and (49) are to be used for the $f^c(x; \mu_{Q_0})$ and $d^c(z; \mu_Q)$ on the first line of Eq. (63). If we drop $O(\alpha_s^2)$ and $O(m^2/Q^2)$ errors, the first line then exactly matches the more standard form of the $O(\alpha_s)$ asymptotic term (see, e.g., Ref. [11]).

The integral that starts on the second line of Eq. (63) is only non-zero at $O(\alpha_s^2)$ or higher, so it may be dropped in a strictly $O(\alpha_s)$ treatment. However, there are several advantages to retaining it. One is simply that it guarantees that, for $Q = Q_0$, we recover the exact asymptotic $k_T \rightarrow Q_0$, $m/Q_0 \rightarrow 0$ limit of the order- α_s^n TMD-term. Another is that it ensures cutoff-invariance through the lowest non-trivial order. Recall that the cutoff-defined pdfs and ffs can in general use a cutoff μ_f that differs from μ_Q . In Eq. (63), μ_f dependence would appear in f^c , d^c , and the Θ functions in the integral of the last three lines. Dependence on μ_f enters the standard asymptotic term at order α_s^2 , but keeping the third term in Eq. (63) ensures that μ_f dependence enters $[f, D]_{\text{ASY}}$ only at order α_s^3 .

VI. EXAMPLE INPUT SCALE TREATMENT

Now we turn to demonstrating how the HSO treatment described in Secs. (II)–(IV) works in practice with explicit numerical implementations. Our purpose here is to compare the HSO treatment described thus far with the conventional steps for constructing phenomenological parametrizations, and to illustrate the improvements that are gained from using the former.

In Sec. VIA below, we will summarize the basic formulas and in Sec. VIB we will review the usual decomposition of a transverse momentum dependent cross section into a TMD term, an asymptotic term, and a Y -term. In Sec. VIC, we will review the conventional style of implementing TMD factorization and show examples of the complications that can arise, some of which were already mentioned in the introduction, and in Sec. VID we show how these are solved within the HSO approach.

In our calculations, we focus on the TMD pdfs and ffs parametrized at an initial scale $Q = Q_0$, a scenario previously addressed in [10]. Estimating the lowest Q_0 for which TMD factorization remains valid is rather non-trivial [16], and we leave it as an open question. For purposes of illustration, we will try two values in sections VIC and VID below, from the relatively low (and reasonable) $Q_0 = 4.0$ GeV, to the (far too conservative) $Q_0 = 20.0$ GeV, to demonstrate how the procedure works for both a small and a large choices of Q_0 .

A. Basic setup

The standard expression for the SIDIS differential cross section in terms of the structure functions F_1 and F_2 is

$$\frac{d\sigma}{dx dy dz dq_T^2} = \frac{\pi^2 \alpha_{\text{em}}^2 z}{Q^2 x y} [F_1 x y^2 + F_2 (1 - y)] , \quad (64)$$

where the F structure functions are the usual ones obtained by contracting the projectors in Eq. (13) with the hadronic tensor. In the small- q_T approximation, the structure functions are expressed in terms of TMD pdfs and ffs,

$$F = F^{\text{TMD}} + O(m/Q, q_T/Q) , \quad (65)$$

$$F_1^{\text{TMD}} \equiv 2z \sum_j |H_j^2 [f_{j/p}, D_{h/j}] , \quad F_2^{\text{TMD}} \equiv 4zx \sum_j |H_j^2 [f_{j/p}, D_{h/j}] , \quad (66)$$

where the “TMD” superscript denotes the small- q_T approximation. Compare Eq. (66) with Eq. (8) for the hadronic tensor. We will use the $O(\alpha_s)$ hard factor $|H_j^2|$ from Eq. (11) in any calculations below. Calculating Eq. (66) in a specific phenomenological implementation involves making choices about how to parametrize the TMD functions $f_{i/p}$ and $D_{h/j}$, including choices about nonperturbative models and/or calculations at the input scale, the order of precision in perturbative parts, and any other approximations or assumptions used in the construction of a specific set of parametrizations.

B. Combining large (F^{FO}) and small (F^{TMD}) transverse momentum calculations

Before we contrast the F^{TMD} calculations in the conventional and HSO styles, let us review the usual steps for merging calculations done with TMDs with purely collinear factorization calculations designed for the $q_T \approx Q$ region.

In the region where $q_T \approx Q$, the approximations in Eq. (66) fail. However, this is the region where fixed-order collinear factorization calculations, which use ordinary collinear pdfs and ffs, are most reliable. We express the large- q_T fixed-order collinear approximation to the structure functions as

$$F = F^{\text{FO}} + O(m/q_T) , \quad F^{\text{FO}} = \sum_{i,j} d_{B/i} \otimes \hat{F}_{ij} \otimes f_{j/p} , \quad (67)$$

where the indices i, j run over parton flavors, and the FO superscript stands for “fixed-order.” A choice must be made for the UV scheme that defines the collinear functions $f_{i/p}$ and $D_{h/j}$. The most common is renormalization in the $\overline{\text{MS}}$ scheme. The \hat{F}_{ij} are the partonic versions of the structure functions, and they have been calculated up to at least $O(\alpha_s^2)$ [52–54]. In our calculations, we will use $O(\alpha_s)$ results [9, 11, 55].

Following standard conventions, we will use the phrase “fixed order cross section” as a short hand for Eq. (64) calculated with the large- q_T approximation in Eq. (67).² While F^{TMD} gives an accurate treatment of the $q_T \approx m$ region, and F^{FO} provides an accurate treatment of the $q_T \approx Q$ region, what is ultimately needed is a factorized expression with only $O(m^2/Q^2)$ -suppressed errors point-by-point in q_T . To construct it systematically, one starts by writing the structure functions in the TMD (low- q_T) approximation with the error term made explicit,

$$F = F^{\text{TMD}} + [F - F^{\text{TMD}}] . \quad (68)$$

The error term in braces is only unsuppressed when q_T is large relative to m . Thus, it can be calculated in collinear factorization with only m^2/q_T^2 -suppressed errors. Since the error term itself is $O(q_T^2/Q^2)$, the result is that the overall error is m^2/Q^2 -suppressed point-by-point in q_T . Thus, we define

$$\lim_{m/q_T \rightarrow 0} F^{\text{TMD}} = F^{\text{ASY}} \quad (69)$$

to be the $q_T \sim Q$, $Q \rightarrow \infty$ asymptote of the TMD approximation, as it is calculated in fixed order collinear factorization. The “ \sim ” means the ratio q_T^2/Q^2 is to be held fixed as $Q \rightarrow \infty$. Applied to Eq. (68), the structure function becomes

$$F = F^{\text{TMD}} + [F^{\text{FO}} - F^{\text{ASY}}] + O(m^2/Q^2) . \quad (70)$$

The asymptotic term is constructed to accurately describe the $m \ll q_T \ll Q$ region – both $q_T \ll Q$ and $m \ll q_T$ approximations have been applied simultaneously. For this paper, this is simply Eq. (63) applied to structure functions.

A minor subtlety is that the exact form of the asymptotic term F^{ASY} depends on the details of how collinear pdfs and ffs are defined and on how higher order corrections in the perturbative expansion are truncated. If, in an $O(\alpha_s^n)$ calculation, for example, the cutoff-defined pdfs and ffs of Eq. (63) are replaced by their corresponding $\overline{\text{MS}}$ definitions, then the resulting asymptotic terms will generally differ by $O(m^2/Q^2)$ -suppressed and $O(\alpha_s^{n+1})$ -suppressed amounts. Furthermore, while F^{ASY} is in principle equal to the low- q_T limit of F^{FO} as $Q \rightarrow \infty$, generally this is only exactly true in calculations at the working order of perturbation theory. In calculations at a fixed Q , the two asymptotic terms will typically differ by higher-order α_s and power-suppressed terms. In other words, if F^{ASY} is calculated to $O(\alpha_s^n)$ with the cutoff scheme for pdfs and ffs, and $F^{\text{FO},r}$ is calculated to the same order in some other scheme r , then one will generally find

$$\left[\lim_{q_T/Q \rightarrow 0} F^{\text{FO},r} \right]^{O(\alpha_s^n)} - [F^{\text{ASY}}]^{O(\alpha_s^n)} = O(\alpha_s^{n+1}, m^2/Q^2) . \quad (71)$$

That is, there is a family of valid schemes for defining the exact asymptotic term at a given order, though some schemes can be preferable to others in the context of minimizing errors. Indeed, it is the first term in Eq. (71), with $r = \overline{\text{MS}}$, that represents the most common approach used in the past for calculating the asymptotic term. We will call the asymptotic term calculated using Eq. (63) $F_{\text{HSO}}^{\text{ASY}}$.

Together, the second two terms in Eq. (70) are often called the “ Y -term,” and the structure function is written as

$$F = F^{\text{TMD}} + Y + O(m/Q) . \quad (72)$$

to emphasize the role of Y as a large- q_T correction to calculations done with TMD pdfs and ffs. Of course, the precise value of the Y -term contribution depends on the specific version of the asymptotic term.

In conventional treatments, the fixed order term is calculated with collinear functions in the $\overline{\text{MS}}$ scheme. The specific version of the asymptotic structure functions used is the first term in Eq. (71), so that

$$F_{\text{ST}}^{\text{FO}} = F^{\text{FO},\overline{\text{MS}}}, \quad F_{\text{ST}}^{\text{ASY}} = \lim_{q_T/Q \rightarrow 0} F^{\text{FO},\overline{\text{MS}}}, \quad (73)$$

with “ST” subscripts to indicate “standard.” We will call a calculation of the asymptotic term done in the style of Sec. V $F_{\text{HSO}}^{\text{ASY}}$ to distinguish it from Eq. (73). Since $F_{\text{HSO}}^{\text{ASY}}$ is calculated with cutoff definitions for the collinear pdfs and ffs, this suggests that the cutoff definitions might be preferred as well for calculating F^{FO} . However, switching between the $\overline{\text{MS}}$ and cutoff schemes in F^{FO} only produces power suppressed and perturbative errors beyond the

² Note that the asymptotic term of Sec. V is also calculated in fixed order perturbation theory. However, in the terminology of this section “fixed order term” applies specifically to calculations done using the non-asymptotic Eq. (67).

working order in α_s . Therefore, one may consistently interchange cutoff and $\overline{\text{MS}}$ definitions, and we will use $F_{\text{ST}}^{\text{FO}}$ for our calculation of the fixed order structure function. We will see in later sections that the effect of switching between the two is small relative to the overall improvements from using the HSO approach. An interesting question for the future is whether calculations of F^{FO} can be improved by switching to a cutoff scheme for the collinear functions, but we leave this to future work.

C. The TMD term in the conventional treatment

The usual approach to applying TMD factorization to phenomenology has been reviewed in many places, so we will not repeat the details here. Readers are referred to, for example, Refs. [3, 56, 57] and references therein. The standard expression used in calculations follow from making the following replacement in Eqs. (66):

$$\begin{aligned} [f_{j/p}, D_{h/j}] &\rightarrow \int \frac{d^2 \mathbf{b}_T}{(2\pi)^2} e^{-i\mathbf{q}_T \cdot \mathbf{b}_T} \tilde{f}_{j/p}^{\text{OPE}}(x, \mathbf{b}_*; \mu_{b_*}, \mu_{b_*}^2) \tilde{D}_{h/j}^{\text{OPE}}(z, \mathbf{b}_*; \mu_{b_*}, \mu_{b_*}^2) \\ &\times \exp \left\{ 2 \int_{\mu_{b_*}}^{\mu_Q} \frac{d\mu'}{\mu'} \left[\gamma(\alpha_s(\mu'); 1) - \ln \frac{Q}{\mu'} \gamma_K(\alpha_s(\mu')) \right] + \ln \frac{Q^2}{\mu_{b_*}^2} \tilde{K}(b_*; \mu_{b_*}) \right\} \\ &\times \exp \left\{ -g_{j/p}(x, b_T) - g_{h/j}(z, b_T) - g_K(b_T) \ln \left(\frac{Q^2}{Q_0^2} \right) \right\}. \end{aligned} \quad (74)$$

The $\tilde{f}_{j/p}^{\text{OPE}}$ and $\tilde{D}_{h/j}^{\text{OPE}}$ on the first line are the TMD pdfs and ffs in b_T -space, expanded and truncated in an operator product expansion. The γ , γ_K and \tilde{K} are the usual evolution kernels. The “ \mathbf{b}_* ” method has been used to regulate $\tilde{f}_{j/p}^{\text{OPE}}$, $\tilde{D}_{h/j}^{\text{OPE}}$, and \tilde{K} at large b_T . (See reviews of the \mathbf{b}_* method in Sec. IXA of [16] and in Sec. VIII of [58].) The most common choice for a functional form for \mathbf{b}_* is

$$\mathbf{b}_*(b_T) = \frac{\mathbf{b}_T}{\sqrt{1 + b_T^2/b_{\text{max}}^2}}, \quad (75)$$

where b_{max} is a transverse size scale that demarcates a separation between large and small transverse size regions. In principle, both the functional form of Eq. (75) and the value of b_{max} are completely arbitrary, but a small b_{max} justifies the use of the OPE on the first line of Eq. (74); the error term in the approximation in Eq. (74) is suppressed by powers of $m b_{\text{max}}$. All of the nonperturbative transverse momentum dependence is contained in the b_T -space functions $g_{j/p}$, $g_{h/j}$, and g_K , whose definitions in terms of the more fundamental correlation functions are

$$-g_{j/p}(x, b_T) \equiv \ln \left(\frac{\tilde{f}_{j/p}(x, \mathbf{b}_T; \mu_{Q_0}, Q_0^2)}{\tilde{f}_{j/p}(x, \mathbf{b}_*; \mu_{Q_0}, Q_0^2)} \right), \quad -g_{h/j}(z, b_T) \equiv \ln \left(\frac{\tilde{D}_{h/j}(z, \mathbf{b}_T; \mu_{Q_0}, Q_0^2)}{\tilde{D}_{h/j}(z, \mathbf{b}_*; \mu_{Q_0}, Q_0^2)} \right), \quad (76)$$

and

$$g_K(b_T) \equiv \tilde{K}(b_*; \mu) - \tilde{K}(b_T; \mu). \quad (77)$$

Conventional methods replace each of the g -functions, $g_{j/p}$, $g_{h/j}$, and g_K , by an ansatz, with parameters to be fitted from measurements. The simplest and most common choices (e.g. [59–61]) are based on simple power laws like

$$g_{j/p}(x, b_T) = \frac{1}{4} M_F^2 b_T^2, \quad g_{h/j}(z, b_T) = \frac{1}{4 z^2} M_D^2 b_T^2 \quad (78)$$

for the input nonperturbative functions, where M_F and M_D are fit parameters. For the CS kernel, common parametrizations are

$$g_K(b_T) = \frac{1}{2} M_K^2 b_T^2 \quad \text{or} \quad g_K(b_T) = \frac{g_2}{2 M_K^2} \ln(1 + M_K^2 b_T^2), \quad (79)$$

where M_K and g_2 are fit parameters. The first of these functional forms is common in typical applications, but it conflicts with the expectation that evolution is slow at moderate Q [62, 63]. As a result, it was suggested in Ref. [56] that $g_K(b_T)$ should exhibit very nearly constant behavior at large b_T , a behavior closely modeled by a logarithmic function. More complex fit parametrization ansatzes for all the g -functions have been introduced more recently (see

for instance Refs. [64, 65]), but the general approach of taking combinations of simple functional forms that reduce to power law behavior at small b_T is similar to the above.

Note that, in the b_* -approach, before any truncation approximations are made, the product of TMD correlation functions must satisfy

$$\frac{d}{db_{\max}} [f_{j/p}, D_{h/j}] = O(mb_{\max}). \quad (80)$$

That is, dependence on b_{\max} or on the form of $\mathbf{b}_*(b_T)$ must be a negligible power correction for reasonably small b_{\max} .³ In calculations at a specific order in α_s , violations of Eq. (80) may enter only through neglected higher orders in α_s . A significant violation of Eq. (80) in a TMD parametrization may indicate either that higher orders need to be included, or that b_{\max} has been chosen to be too large. A failure to find a negligible right side of Eq. (80) is thus a useful diagnostic tool.

We will label structure functions calculated in the conventional approach by $F_{\text{ST}}^{\text{TMD}}$, with “ST” for “standard,” and we will use this notation regardless of whichever specific model is used for the g -functions. What makes an approach “conventional” in the sense that we mean in this paper is that it imposes no extra, additional constraints on the g -functions to ensure consistent matching with collinear factorization. Specifically, the ansatzes of traditional approaches do not explicitly enforce the integral connection between collinear and TMD pdfs and ffs in Eq. (2), or guarantee a smooth interpolation to the large k_T collinear factorization region.

In the following numerical examples, we will use CTEQ6.6 pdfs [66] (central values) and MAPFF1.0 ffs for π^+ [67] (average over replicas), implemented in LHAPDF6 [68]. We postpone a more detailed analysis that includes the uncertainty associated with the chosen LHAPDF6 sets for a later publication. For the purpose of this paper, we effectively assume “complete knowledge” of the collinear pdfs and ffs in the $\overline{\text{MS}}$ scheme stressing that our main points, and the logic behind the HSO approach, are not affected by such choices. The left-hand panels of Fig. 2 show the differential SIDIS cross section for $Q_0 = 4.0$ GeV within the various different approximations discussed in Sec. VIA and Sec. VIB, including the $F_{\text{ST}}^{\text{TMD}}$ (the TMD approximation), the $F_{\text{ST}}^{\text{FO}}$ ($q_T \approx Q$ approximation), and the $F_{\text{ST}}^{\text{ASY}}$ (asymptotic term) calculations. We use $x = 0.1$, $z = 0.3$ and $y = 0.5$, which are kinematics accessible to both the COMPASS experiment [8] and the EIC [69]. To emphasize alternately the large- q_T and small- q_T regions, we have plotted the curves on a logarithmic scale in the upper left panel and a linear scale in the lower left panel. We take the g -functions to be parametrized as in Eq. (78), and the RG scale is $\mu_{Q_0} = Q_0$. The curves are the TMD (solid red line), fixed order (dot-dashed black line) and asymptotic (dashed blue line) terms. Despite the small values used for the mass parameters, $M_F = M_D/z = 0.1$ GeV, the asymptotic term is nowhere close to overlapping with either the TMD or the fixed order terms anywhere in the range of q_T between 0 and 4 GeV. This is a violation of the consistency requirement that, with a sufficiently large input scale Q_0 , there must be a region $\Lambda_{\text{QCD}} \ll q_T \ll Q_0$ where the asymptotic term is simultaneously a good approximation of both the TMD and the $q_T \approx Q_0$ fixed order cross sections. This is a complication that arises frequently in the conventional methodology, and it is one that we alluded to in Sec. I. Among the reasons for the mismatch is a failure to impose the integral relation in Eq. (2) directly upon the g -functions in Eq. (78).

One might suspect that the mismatch is a consequence of the input scale Q_0 being too small. To test this, we also consider the same computation, using the same nonperturbative mass scales, but now with an unreasonably large input scale of $Q_0 = 20$ GeV. The result is shown in the right-hand panels of Fig. 2. Again, the upper panel is on a logarithmic scale, while the lower panel uses the linear scale to emphasize the region of smaller q_T . The agreement between the asymptotic and TMD terms improves, but even here there is a startlingly large mismatch between the three calculations in the region where q_T is small but comparable to Q_0 . Even for $Q_0 \approx 20$ GeV, there is no region of q_T where the three curves overlap simultaneously to a satisfactory degree. This point is made especially clear in the linear scale plots.

Note that this complication is independent of evolution or the question about how many orders of logarithms of Q/q_T should be resummed. If the connection to collinear factorization is to be consistent, there must be a region where q_T is a fixed fraction of Q and all three calculations merge in the limit as $Q \rightarrow \infty$. Moreover, for any Q where we expect TMD factorization to be valid, the TMD and asymptotic terms should at least approximately match one another when q_T is comparable to Q . It is a contradiction, then, if this fails at the input scale. Note that the mismatches, both quantitative and qualitative, between the TMD terms and their expected asymptotic behavior is especially visible in the lower panels where the curves are plotted with linear axes.

³ The power-suppressed errors on the right side of Eq. (80) will typically be $m^2 b_{\max}^2$, but the precise power of the suppression is not important for our present discussion.

For generating the plots in Fig. 2, it was necessary to fix the mass scales M_F and M_D in Eq. (78). The observed trends are quite general, however, and to demonstrate this we show the same $Q_0 = 4.0$ GeV calculation in the left-hand panel of Fig. 3, but now with bands representing ranges of typically-sized nonperturbative mass scales,

$$0.1 \text{ GeV} \leq M_F \leq 0.4 \text{ GeV}, \quad (81)$$

$$0.1 \text{ GeV} \leq M_D/z \leq 0.3 \text{ GeV}. \quad (82)$$

The value of b_{\max} for this plot remains fixed at 1.0 GeV^{-1} . Even with the freedom to adjust these nonperturbative parameters, it is clear that it is not possible to achieve reasonable agreement between the TMD term and the asymptotic term, even in regions where q_T is comparable to Q_0 . The TMD bands do touch the asymptotic curve at around $q_T \approx 0.5 \text{ GeV}$, but the two curves have very different qualitative shapes for all M_D and M_F . For larger q_T , there is no approximate agreement between the asymptotic and TMD terms, regardless of M_F and M_D . Indeed, the TMD band departs from the asymptotic term at around $q_T \approx 1.2 \text{ GeV}$.

Another way to see the problems with the conventional treatment here is to observe that the approximate b_{\max} -independence of Eq. (80) is very badly violated with typical values of b_{\max} , as shown by the right-hand panel in Fig. 3, which displays the TMD term with bands for b_{\max} variations from the very small value of 0.1 GeV^{-1} up to a maximum typical value of $b_{\max} = 1.5 \text{ GeV}^{-1}$ used in phenomenological applications. The bands are with fixed mass scales of $M_F = M_D/z = 0.25 \text{ GeV}$. The orders-of-magnitude variation badly contradicts the original b_{\max} -independence that exists before the OPE approximations. It implies that the M_F and M_D parameters must be given their own b_{\max} -dependence to (at least approximately) cancel the explicit b_{\max} -dependence seen in the figure. However, the far more modest M_F and M_D dependence seen in the left-hand panel shows that this cannot be made to work with typical model parametrizations of the g -functions and reasonable nonperturbative values for M_F and M_D .

As a consequence of the strong b_{\max} sensitivity, practical phenomenological applications will often effectively promote b_{\max} to the status of an extra nonperturbative parameter as opposed to treating it as an entirely arbitrary cutoff. That is, attempts to approximately preserve Eq. (80) are effectively abandoned. But the result is that the large transverse momentum behavior becomes sensitive to parameters that are in principle to be restricted to describing only the nonperturbative small transverse momentum region. The predictive power that is gained from collinear factorization and the OPE is then compromised. This is a problem that has been well-known for some time [18].

The above observations illustrate that nonperturbative transverse momentum dependence in the conventional methodology has an unacceptably large impact on the large transverse momentum region, in a way that violates consistency with collinear factorization.

D. In a hadron structure oriented approach

Next, we contrast the conventional approach of the preceding subsection with the HSO steps from Ref. [16] and Secs. (II)–(V) of this paper.

It should be emphasized that the two “approaches” being contrasted here refers only to specific phenomenological implementations and not to the basic theoretical setup. The fundamental TMD factorization theorem and the evolution equations are always the standard ones, and they are never modified. What distinguishes the HSO approach to phenomenological implementations from the conventional one is that the former imposes constraints on the input TMD parametrizations that guarantee consistency with collinear factorization in the appropriate limits. To see what this means more clearly, it may be helpful to recall that it is straightforward (though unnecessary) to use the \mathbf{b}_* method to rewrite the HSO expression in Eq. (15) in terms of the g -functions defined in Eq. (76), but with the explicit HSO parametrizations for $\tilde{f}_{j/p}(x, \mathbf{b}_T; \mu_{Q_0}, Q_0^2)$ and $\tilde{D}_{h/j}(z, \mathbf{b}_T; \mu_{Q_0}, Q_0^2)$. The final form of the evolved TMD pdfs and ffs are exactly the same. The full set of steps for translating the HSO approach into the conventional one may be found in Sec. IX of [16]. Cast in this way, the HSO approach is identical to the conventional one except that it imposes additional and important consistency conditions directly on the g -functions. In the treatment in this paper, this amounts to using Eq. (17), Eq. (18) and Eq. (28) (or, more generally, any other set of parametrizations that arise from the steps in Ref. [16]) inside Eqs. (37)–(38) instead of the conventionally unconstrained ansatzes like Eqs. (78)–(79).

We have focused on the kinematics of the $Q \approx Q_0$ region, since the lowest acceptable values of Q are where one typically expects nonperturbative hadron structure effects to be most pronounced, and thus it is where nonperturbative versions of relations like Eq. (1) and Eq. (2) become especially important.

The steps for calculating the TMD term in the HSO approach were reviewed in Secs. (II)–(IV). If we specialize to the additive structure in Sec. III for the TMD parametrizations, then the HSO approach amounts to simply calculating

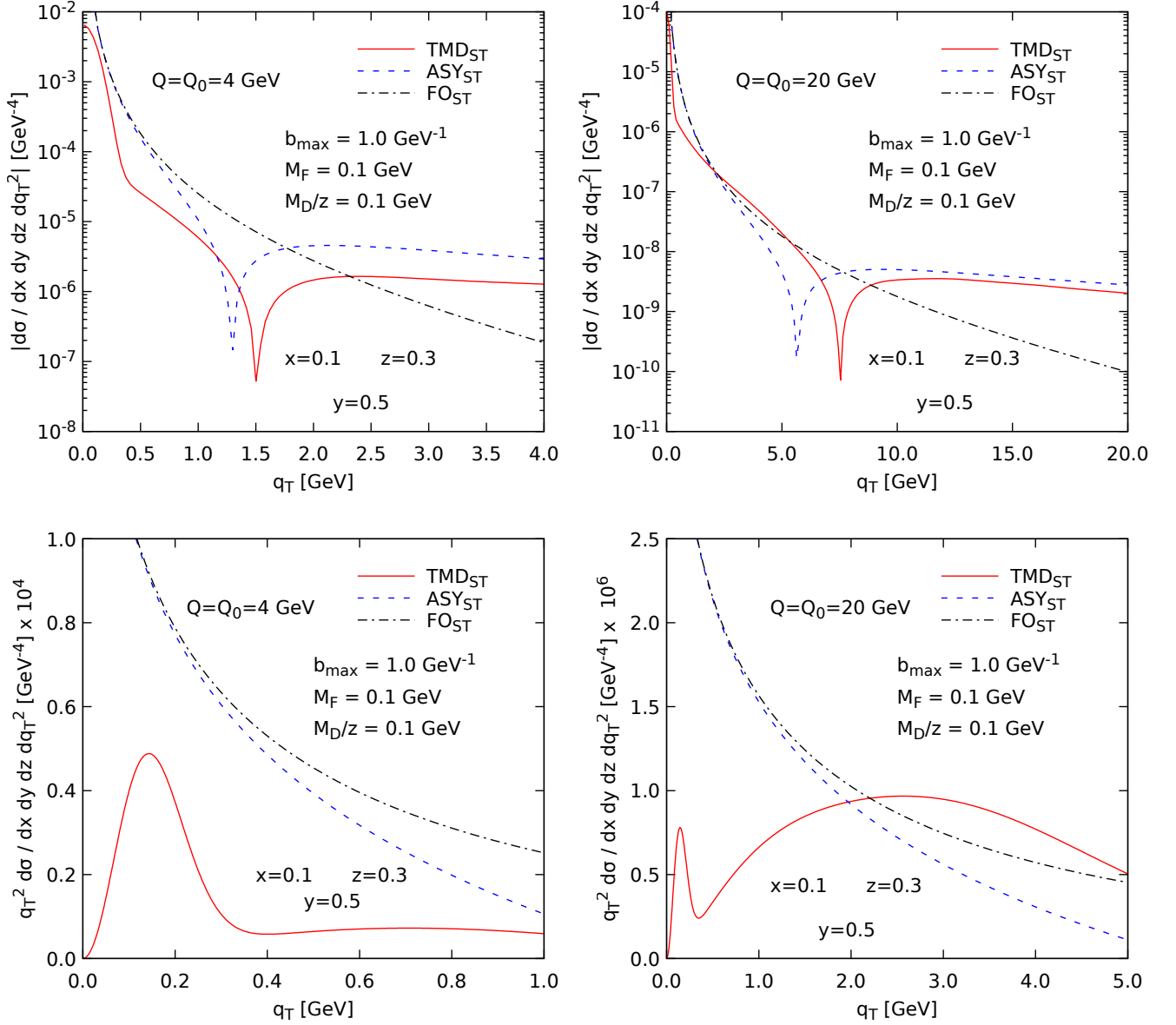


FIG. 2: SIDIS differential cross section (absolute value) in the standard approach, within different approximations for the structure functions: F_{ST}^{TMD} (solid red line), F_{ST}^{ASY} (dashed blue line) and F_{ST}^{FO} (dot-dashed black line). The chosen kinematics roughly correspond to regions accessible by the COMPASS experiment and the EIC. The TMD term is calculated with the quadratic model for the g -functions of Eq. (78), at fixed values for the small-mass parameters $M_F = M_D/z = 0.1$ GeV, and we have used the b_* prescription of Eq. (75) with $b_{\max} = 1.0$ GeV $^{-1}$. We consider the cross section at two values of the input scale Q_0 , and no TMD evolution is performed. Left: The cross section is shown for $Q_0 = 4.0$ GeV. Right: The cross section is shown for $Q_0 = 20.0$ GeV. For visibility, the bottom panels show the same curves as the top, but with a vertical linear scale and a reduced range of q_T . Note that, despite the small values of the mass parameters, the three approximations never overlap in the intermediate region of transverse momentum, $m \ll q_T \ll Q$.

Eq. (15) with the parametrizations in Eq. (18) and Eq. (28). That is, we use

$$\begin{aligned}
 [f_{j/p}, D_{h/j}] &\rightarrow \int \frac{d^2 \mathbf{b}_T}{(2\pi)^2} e^{-i\mathbf{q}_T \cdot \mathbf{b}_T} \tilde{f}_{j/p}(x, \mathbf{b}_T; \mu_{Q_0}, \mu_{Q_0}^2) \tilde{D}_{h/j}(z, \mathbf{b}_T; \mu_{Q_0}, \mu_{Q_0}^2) \\
 &\times \exp \left\{ \tilde{K}(b_T; \mu_{Q_0}) \ln \left(\frac{Q^2}{Q_0^2} \right) + \int_{\mu_{Q_0}}^{\mu_Q} \frac{d\mu'}{\mu'} \left[2\gamma(\alpha_s(\mu'); 1) - \ln \frac{Q^2}{\mu'^2} \gamma_K(\alpha_s(\mu')) \right] \right\}, \quad (83)
 \end{aligned}$$

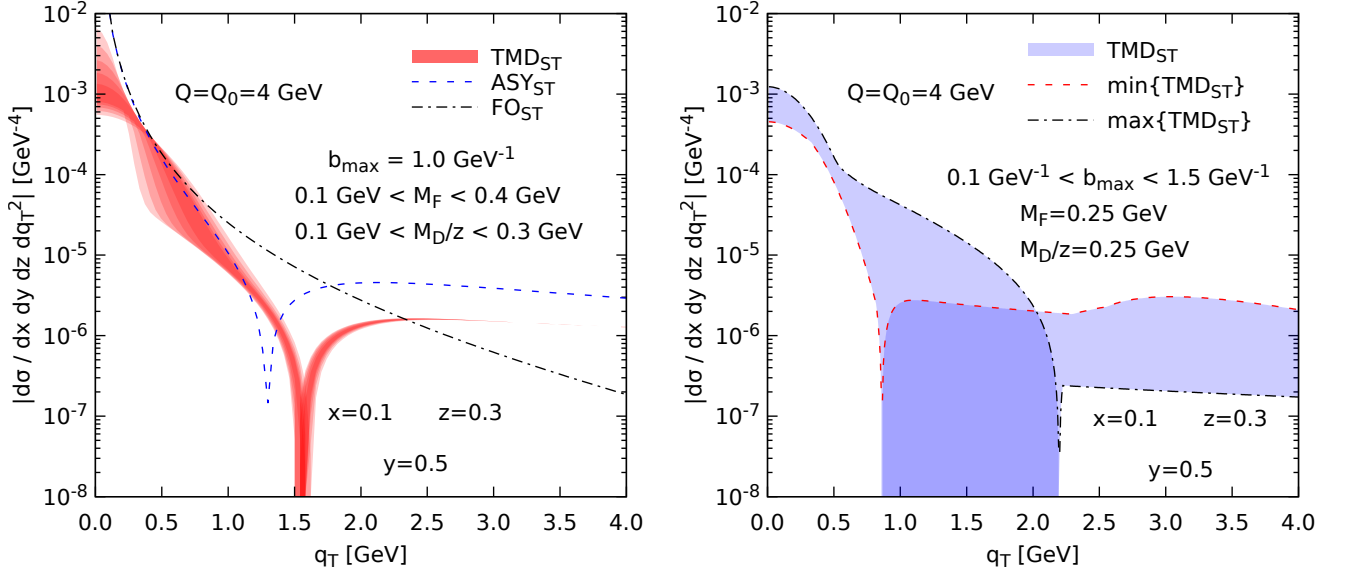


FIG. 3: Variation of the TMD cross section (absolute value), in the standard approach, with respect to the small-mass parameters of Eq. (78) (left), and b_{\max} (right). In both cases, we have chosen the same kinematics as in the left panel of Fig. 2, and we have set $Q = Q_0 = 4.0 \text{ GeV}$, and no TMD evolution is performed. Left: the red band shows the envelope for the TMD term obtained by varying the model masses M_F and M_D . Note the large variation of the band in the region where the asymptotic term (dashed blue line) and the fixed order term (dot-dashed black line) start to overlap, which results from the unconstrained behavior of the TMD term at large q_T . At very large values of q_T , the TMD and asymptotic terms are not consistent. Right: Envelope showing the variation of the TMD term (blue band) with respect to the value of b_{\max} , at fixed values of the model masses. (Note that the edges of the envelope are not necessarily the curves associated with the extrema of the chosen range for b_{\max}). The strong b_{\max} dependence results from the lack of constraints on the models for the g-functions in our example. This dependence persists even in the region $q_T \sim Q$, where the OPE should in principle determine the behaviour of the TMD cross section.

with Eqs. (66). In the replacement, the $\tilde{D}_{h/j}$ and $\tilde{f}_{j/p}$ are now to be understood to be the b_T -space version of the parametrizations from Eq. (18) and Eq. (28) substituted into Eqs. (37)–(39). Explicit expressions for the input b_T -space TMD functions are listed in Appendix B. We denote the resulting structure functions by $F_{\text{HSO}}^{\text{TMD}}$. These are the underlined correlation functions from [16]⁴, or, if we restrict $Q \approx Q_0$ and use the approximation in Eq. (40), they are just the b_T -space input functions themselves. With $O(\alpha_s)$ perturbative coefficients, their structure is

$$F_{\text{HSO}}^{\text{TMD}} \sim (|H_j^2|)^{O(\alpha_s)} [f_{j/p}, D_{h/j}], \quad (84)$$

where $(|H_j^2|)^{O(\alpha_s)}$ is the hard coefficient in Eq. (11), with kinematic factors and sums over flavors.

For the asymptotic term, we start from $F_{\text{HSO}}^{\text{TMD}}$ and use the $m \ll q_T \ll Q$ approximation in Eq. (63) in place of $[f, D]$, so that the asymptotic structure functions are

$$F_{\text{HSO}}^{\text{ASY}} \sim (|H_j^2|)^{O(\alpha_s)} [f_{j/p}, D_{h/j}]_{\text{ASY}}. \quad (85)$$

For calculating the $O(\alpha_s)$ fixed order structure function in $q_T \approx Q_0$ collinear factorization (see, for example, Ref. [54]), we use

$$\frac{(|H_j^2|)^{O(\alpha_s)}}{e_j^2} F_{\text{ST}}^{\text{FO}} = F_{\text{ST}}^{\text{FO}} + O(\alpha_s (\mu_{Q_0})^2), \quad (86)$$

⁴ Actually, these symbols refer to a class of models for the TMD pdfs and ffs since at this stage we still need to specify the exact form of the nonperturbative transverse momentum dependence in $f_{\text{core},i/p}$ and $D_{\text{core},h/j}$. We will use the same notation for all calculations that use this general approach.

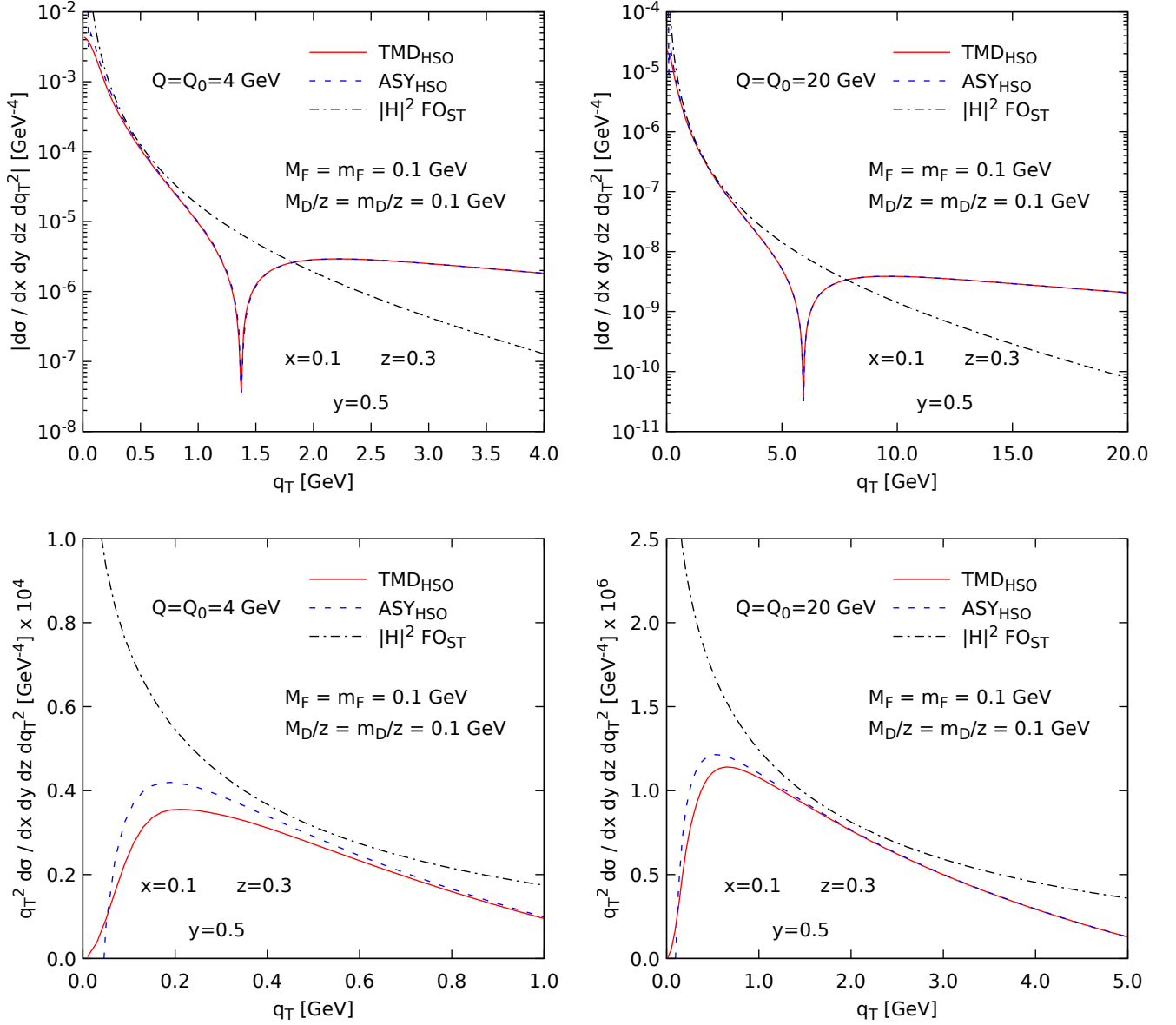


FIG. 4: SIDIS differential cross section (absolute value) in the HSO approach, comparing different approximations for the structure functions: $F_{\text{HSO}}^{\text{TMD}}$ (solid red line), $F_{\text{HSO}}^{\text{ASY}}$ (dashed blue line) and F^{FO} as in Eq. (86) (dot-dashed black line). For comparison, the same kinematics have been used as in Fig. 2. The TMD term is calculated with the Gaussian models of Eqs. (43)–(50), with appropriate constraints as in Eq. (18) and Eq. (28). These models essentially determine the g -functions, similar to Eq. (78) in the standard approach, but with the correct treatment of the large- k_T behavior and the implementation of integral relations. To allow for a meaningful comparison, we use the same values for the small-mass parameters $M_F = M_D/z = 0.1$ GeV as in Fig. 2. The masses appearing in Eq. (18) are set to $m_{D_{h,j}} = m_{D_{h,g}} = M_D$, and those in Eq. (28) to $m_{f_{i,p}} = m_{f_{g,p}} = M_F$. We compute the cross section at the same two values for the input scale Q_0 considered in Fig. 2. Left: The cross section for $Q_0 = 4.0$ GeV. Right: The cross section for $Q_0 = 20.0$ GeV. Note the improvement in the consistency of the three terms, even at $Q = Q_0 = 4.0$ GeV in the left panels, with respect to the standard approach shown in Fig. 2. As larger Q_0 are considered (e.g., with the larger scale $Q_0 = 20$ GeV above) the three curves begin to converge in the $m \ll q_T \ll Q_0$ region.

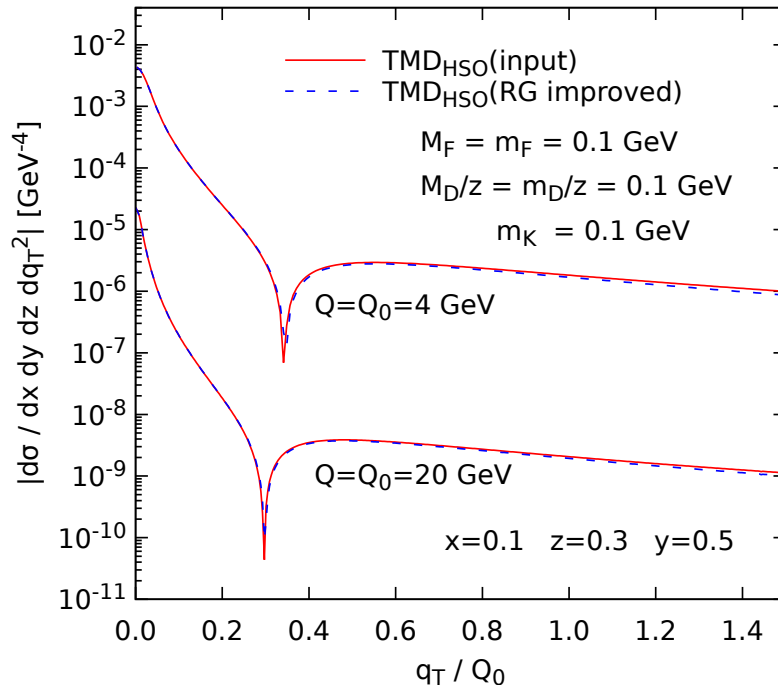


FIG. 5: Comparison of the two versions of the HSO approach discussed in the text, at the two values of the input scale considered, $Q_0 = 4.0$ GeV and $Q_0 = 20.0$ GeV. The red solid lines show the TMD term calculated directly with the input functions of Eq. (18) and Eq. (28), as it was done in our examples in Fig. 2 and Fig. 6. The blue dashed lines show the TMD term in the HSO approach but with renormalization group (RG) improvement (the underline version of functions from Ref. [16]) applied at very small b_T , implemented in Eqs. (37)–(39), with the transition function \bar{Q}_0 of Appendix A. In the HSO approach, for $Q \approx Q_0$, these RG improvements affect only the large q_T region of the cross section. For our examples in this article, even for $q_T/Q_0 \approx 1.5$, differences are not significant.

where F_{ST}^{FO} are the \overline{MS} structure functions of Eq. (67). Keeping the overall factor in F_{ST}^{FO} does not formally change the treatment at the $O(\alpha_s)$ level, but retaining it improves the agreement with the asymptotic term of Sec. V in the $m \ll q_T \ll Q_0$ limit.

We show numerical examples of F_{HSO}^{TMD} , F_{HSO}^{ASY} and F^{FO} in Fig. 4, calculated using the Gaussian models of Eq. (43) in Eq. (18) and Eq. (28). The kinematics are the same as in Fig. 2, and the nonperturbative parameters take the values

$$M_F = M_D/z = 0.1 \text{ GeV}, \quad (87)$$

so that our treatment of the nonperturbative contribution is comparable to the conventional treatment in Fig. 2. Aside from the transition to a tail region, the Gaussian model mimics the power-law behavior of g -functions in Eq. (76) with Eq. (78) for the conventional approach. As in Fig. 2, we show the case of a lower input $Q_0 = 4.0$ GeV in the left panels of Fig. 4, and a large $Q_0 = 20.0$ GeV in the right panels. The upper two panels show the plots on a logarithmic scale to magnify the improvements at large transverse momentum. To magnify the effect of the improvement on the small transverse momentum region, we have replotted the same graphs on linear vertical axes and over a smaller q_T range in the lower two panels. The qualitative and quantitative improvements of the HSO over the conventional approach are especially visible on the linear axes. For these calculations we have used the approximation $\bar{Q}_0 \rightarrow Q_0$ in Eqs. (37)–(38) because this allows us to utilize the analytic expressions for the TMD pdf and ff parametrizations. We confirm in Fig. 5, however, that the effect of the evolution factor is negligible at the input scale. This is by design; the evolution factor is only relevant for evolving to Q well above the input scale.

Comparing Fig. 4 with Fig. 2 confirms that, in terms of maintaining consistency with the collinear factorization region, there is a very substantial improvement with the HSO approach as compared with the conventional approach. For $Q_0 = 4.0$ GeV, the TMD and asymptotic terms match nearly exactly for all $q_T \gtrsim 0.5$ GeV up to Q_0 . There is also a region around $q_T \approx 0.5$ GeV where all three calculations smoothly overlap. Notice also that the region of overlap becomes better defined when going from the left panel (low input scale) to the right panel (high input scale)

of Fig. 4. And, with the larger Q_0 , the agreement between the TMD and asymptotic terms is nearly exact over the whole visible range of q_T . Thus, the HSO plots exhibit the expected trends when choosing larger or smaller values of Q_0 . Of course, the calculations with Q_0 as large as 20 GeV are not physically sensible, but they confirm that the two ways of computing the mid- q_T behavior (with asymptotic and TMD terms) are compatible and consistent in the limit of a fixed q_T/Q_0 ratio and large Q_0 .

From Fig. 3, it is clear that in order to correct the large- q_T behavior of the TMD-term in the conventional methodology to recover the asymptotic term, one would need to make further adjustments to the nonperturbative, non-tail part of the parametrization. But it would have to be done in a way that allows nonperturbative transverse momentum parameter dependence to propagate to unacceptably large q_T . That could be through both explicit nonperturbative parameters like M_F and M_D and through the residual dependence on b_{\max} . In order to reduce the b_{\max} dependence at large q_T to acceptable levels while forcing the TMD and asymptotic terms to converge in Fig. 3, one would have to allow dramatic dependence on nonperturbative parameters that affects the behavior at unacceptably large transverse momentum. To illustrate that the HSO approach addresses this problem, we plot the HSO structure functions, again at the input scale, $Q = Q_0 = 4.0$ GeV, but now with both the Gaussian models of Eq. (43) and the spectator diquark models of Eq. (44), and with the same ranges of values of the nonperturbative mass parameters as were used in the conventional treatment. In the HSO approach, there is no b_* or b_{\max} , and the TMD and asymptotic terms converge toward one another automatically. The results are shown in Fig. 6, with red bands showing the effect of adjusting the nonperturbative mass parameters in the range of Eqs. (81)–(82), and with the Gaussian model in the left-hand panel and the spectator diquark model in the right-hand panel. In each case, we also display the HSO asymptotic (dashed blue line) and fixed order terms (dot-dashed black line).⁵ To see the improvement brought about by the HSO approach, these plots should be compared with the analogous plot in Fig. 3 of the conventional treatment.

The small- q_T regions in both of the cases shown in Fig. 6 exhibit the behavior of their respective nonperturbative models. As q_T grows, the red bands around the TMD curves converge around the asymptotic term, until the the TMD and asymptotic curves are indistinguishable, independently of the nonperturbative model or the values used for M_D and M_F . This illustrates how the HSO approach enforces a smooth transition to a region that is insensitive to the value of nonperturbative transverse momentum dependence parameters. Even with the spectator model on the right, where the TMD curves come with visible bands close to the zero node, the curves still match the general shape of the asymptotic term down to $q_T \approx 0.5$ GeV. The HSO approach ensures this type of behavior.

With the Gaussian model in the left-hand panel Fig. 6, the bands show that agreement between the TMD term and the asymptotic term in the region of $q_T \approx 0.5$ to ≈ 1.0 GeV requires that the mass parameters be kept rather small. For spectator model, the right-hand plot shows that there is more flexibility to adjust the nonperturbative parameters without spoiling approximate agreement with the asymptotic term at mid q_T .

In Fig. 4 and Fig. 6, we also plotted the $q_T \approx Q$ fixed order curves to show its approximate overlap with the asymptotic and TMD terms in a region of mid q_T . In these calculations, we used $\overline{\text{MS}}$ pdfs and ffs. As mentioned in the discussion after Eq. (73), it may turn out to be preferable to use the cutoff definitions for the collinear functions to match what is done with the asymptotic term. For the purposes of this paper, however, the difference between the two is small enough to ignore, as can be seen in Fig. 7 where we plot the ratios of the collinear pdfs and ffs defined with the cutoff scheme and the $\overline{\text{MS}}$ scheme. For the ranges of x and z that we have consider in this paper, the difference between the schemes is $\lesssim 10\%$, which is comparable to the spread between the asymptotic and fixed order curves in Fig. 4. It is perhaps interesting that the switch from the $\overline{\text{MS}}$ to the cutoff pdfs tends to move the fixed order curve closer to the asymptotic curve. However, we leave the question of whether switching to all cutoff definitions can improve the treatment to future work.

The above style of analysis can be applied directly to the individual TMD correlation functions instead of the full structure functions, and this may be a preferred way to organize the discussion in contexts where understanding the role of hadron structure is the primary goal. In particular, given a nonperturbative treatment of the small k_T region of a TMD pdf or ff, we may confirm that the TMD function matches its order α_s^n tail at $k_T \approx Q_0$. An example is shown in Fig. 8 for the Gaussian core model. The bands show the effect of varying the mass parameters as in the left panel of Fig. 6, calculated as in Eq. (18) and Eq. (28). The correlation functions are the TMD pdf of up-quarks in a proton (left panel), and the TMD ff of up-quarks into π^+ (right panel). (These are exactly the functions used in the cross section of Fig. 6.) The dot-dashed lines are the corresponding perturbative calculations in Eq. (41) and Eq. (42). These are the “asymptotic terms,” analogous to the dashed curves in Fig. 4, but corresponding to the separate TMD correlation functions. The plots show that, regardless of the nonperturbative treatment of small

⁵ Since $F_{\text{HSO}}^{\text{ASY}}$ is calculated with cutoff collinear functions, they also depend on the values of the mass parameters and should in principle be also displayed as bands in Fig. 6. However, the variations are negligibly small for the ranges of the mass parameters considered here, so for visibility we show only central lines instead.

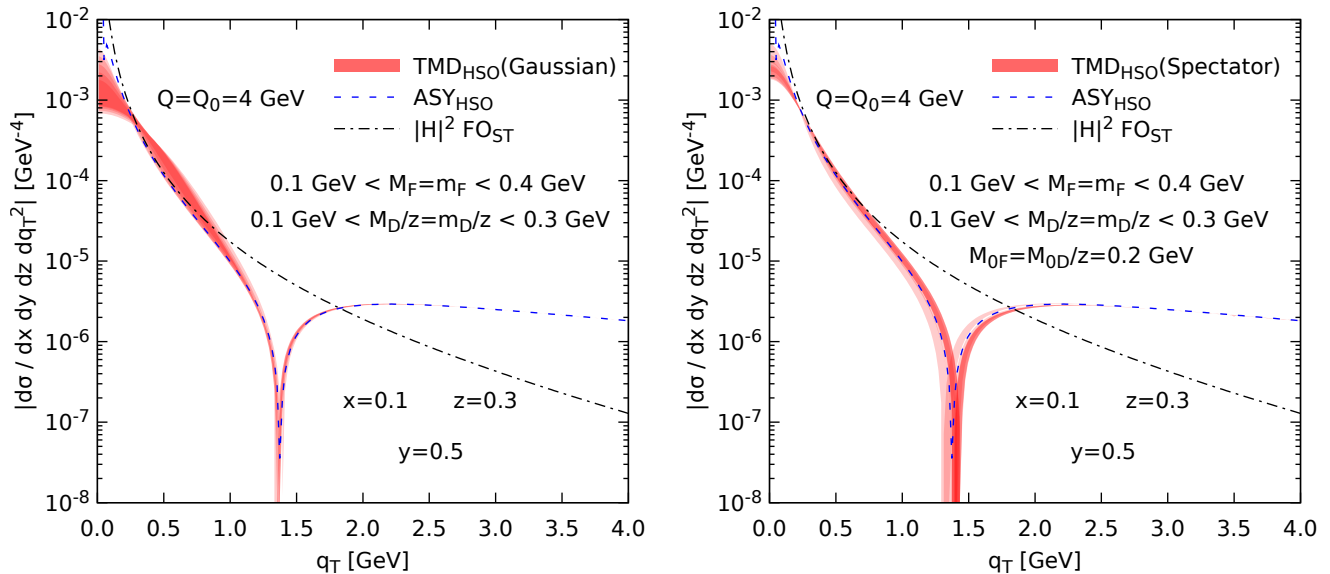


FIG. 6: Variation of the TMD cross section (absolute value), in the HSO approach, with respect to small-mass parameters (red bands). The same kinematics as in the left panel of Fig. 3 have been used, so that $Q = Q_0 = 4.0$ GeV and no TMD evolution is performed. For visibility, we display only the central lines of the corresponding cross sections with the $F_{\text{HSO}}^{\text{ASY}}$ (dashed blue line) and F^{FO} as in Eq. (86) (dot-dashed black line) approximations, since their variation with the small masses is very mild. Left: calculation with the Gaussian ansatz of Eq. (43), obtained by varying the model masses M_F and M_D ; this is the constrained version of the quadratic models for the g-functions of Eq. (78), in the standard approach. Right: implementation of the spectator model Eqs. (44)–(45) in the HSO approach. In each case, the HSO approach ensures the consistency of the initial models for TMDs and collinear factorization calculations. Note that our prescription can be readily applied to any other model.

k_T , the TMD correlation functions treated in this way are always consistent with their $k_T \approx Q_0$ behavior, found in collinear factorization, starting at around $q_T = 1.0$ GeV. The analogous plots for other flavors exhibit similar trends.

VII. CONCLUSION

Let us conclude by summarizing the primary results of the last section: We have shown how to implement TMD factorization to calculate unpolarized SIDIS cross sections at an input scale Q_0 in a way that centers the role of nonperturbative calculations of hadron structure, and we have shown how this leads to a dramatic improvement in the consistency between TMD and collinear factorization, particularly near the input scale Q_0 . Our approach, which we have called a “hadron structure oriented” approach in this paper, and which is based upon the setup in [16], imposes additional constraints beyond what is standard in the more conventional style of implementing TMD factorization, reviewed above in Sec. VI C. These extra constraints are designed especially to preserve a TMD parton model interpretation (in the sense of preserving Eq. (1)) for small transverse momentum behavior while ensuring a consistent transition to collinear factorization at $q_T \approx Q_0$ and $Q_0 \gg \Lambda_{\text{QCD}}$. We have emphasized throughout that it is straightforward to swap the parametrization of the nonperturbative core of a TMD pdf or ff in the HSO approach, so that any preferred model or nonperturbative technique for describing the small transverse momentum region may easily be incorporated into future implementations. We highlighted this modular feature of the HSO approach by exchanging a Gaussian model for a spectator diquark model in Fig. 6; replacing one description of the nonperturbative core by another leaves the $q_T \approx Q_0$ region of the TMD term unaffected and consistent with large- q_T collinear factorization.

Of course, there are still other open questions with regard to the domain of applicability of TMD factorization to processes like SIDIS. For example, a definitive lowest value for Q (for each x and z) in SIDIS below which TMD factorization techniques absolutely cease to be useful remains to be determined. It is likely that a sharp transition does not exist. A related question is that of how high q_T may become before the TMD term alone is no longer sufficient, and the description must transition into a $q_T \approx Q$ region where TMD factorization fails and one must rely entirely on fixed order collinear factorization. (This is the issue of the “Y-term” alluded to in the introduction.)

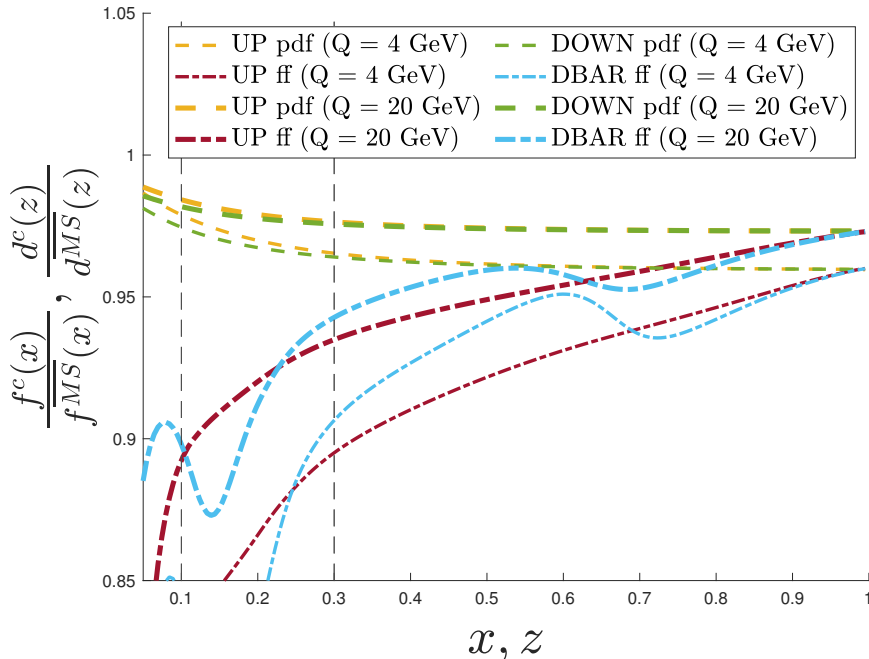


FIG. 7: Ratio of the cutoff definitions of both collinear pdfs (dashed) and ffs (dot-dashed) and their $\overline{\text{MS}}$ counterparts. The results are shown for two values of the hard scale $Q \in \{4, 20\}$ GeV. Only the flavors that contribute most to the cross section under consideration have been shown to facilitate the readability of the plot. The cutoff has been chosen to match the hard scale, i.e. $k_c = Q$ with the choice of the Gaussian model for TMDs for the “core” parametrization of both pdfs and ffs. Notice that any other choices for the “core” model or the nonperturbative mass parameters would only affect the result with power suppressed contributions which, if neglected, make the difference between the two schemes perturbatively calculable as in the last term in Eq. (22) (ff) and Eq. (32) (pdf). The dashed black lines correspond to the choices of $x = 0.1$ and $z = 0.3$ made in our computations throughout the paper. Replacing the two definitions thus accounts for a difference of order $\sim 3\%$ ($Q = 4$ GeV) to $\sim 2\%$ ($Q = 20$ GeV) for the pdf case and $\sim 10\%$ ($Q = 4$ GeV) to $\sim 5\%$ ($Q = 20$ GeV) for the ff case.

Below some numerical value of Q , it is no longer meaningful to separate a cross section into distinct large ($q_T \approx Q$) and small ($q_T \approx \Lambda_{\text{QCD}}$) transverse momentum regions. These should probably be viewed as open empirical questions, to be confronted by future experimental tests. But posing them in a clear way requires unambiguous and internally consistent steps like those we have described here and in [16] with the HSO approach.

A separate phenomenological issue is that one generally finds tension between data for large transverse momentum in processes like SIDIS and Drell-Yan scattering and calculations performed with existing collinear pdf and ff fits [14, 53, 54, 70]. This suggests that it will be important for future phenomenological efforts to fit TMD and collinear functions simultaneously in a full TMD factorization context. Of course, for this to be meaningful the nonperturbative parts need to be combined with collinear factorization in a consistent procedure, and this is what the HSO approach is meant to provide.

Extending the treatment in this paper of SIDIS to other processes like Drell-Yan scattering is straightforward. Moreover, order α_s^2 and even α_s^3 versions of the parametrizations are obtainable from straightforward, albeit somewhat cumbersome, translations of existing results. It will ultimately be necessary as well to formulate the spin and azimuthal dependent observables in TMD factorization in a manner analogous to what we have done here for the unpolarized case. There, interesting subtleties arise from matches and mismatches between small and large transverse regions of the TMD pdfs and ffs [71–73]. In addition, there exist other QCD formalisms that invoke the notion of a TMD or unintegrated parton density and find complications with preserving relationships like Eq. (1), see for example Refs. [74, 75] and the discussion in Refs. [76–78]. We hope that our work might provide some input in resolving these problems. Finally, it bears mentioning that the HSO approach that we advocate here is entirely compatible with other frameworks for setting up TMD factorization and/or transverse momentum resummation methods, including soft-collinear effective theory based approaches [79–84].

For our next steps, we plan to perform explicit phenomenological extractions within the HSO approach discussed here. It has the advantage of placing us in a position to systematically analyze the contributions from any nonperturbative models (e.g., the spectator model) for the small transverse momentum region separately from the large

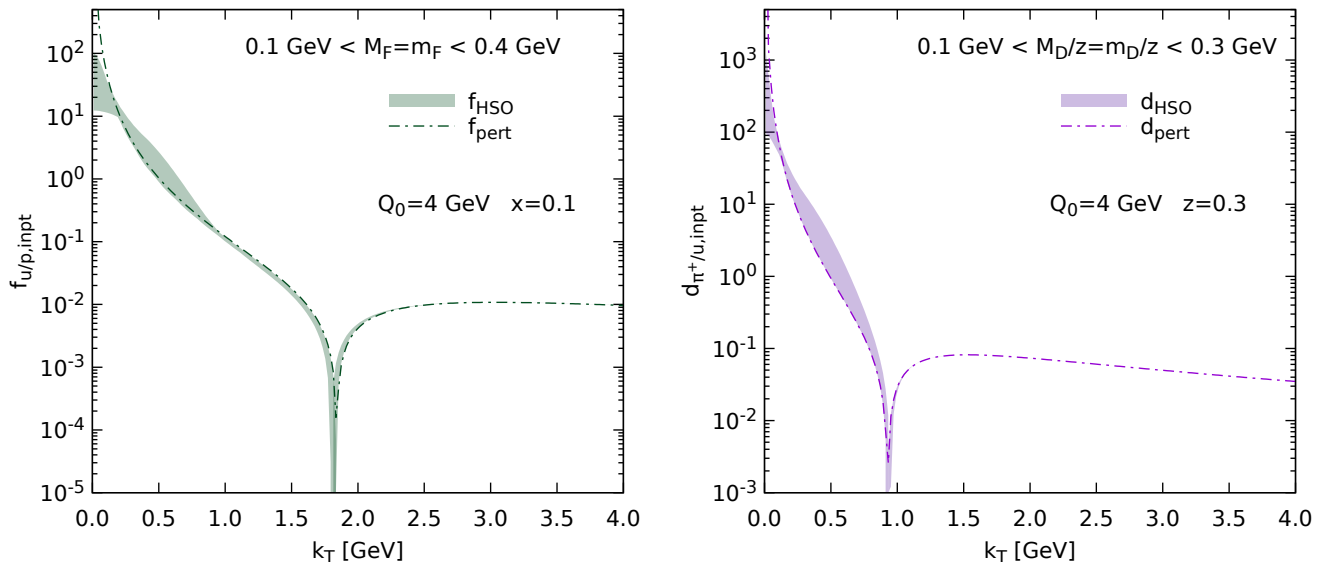


FIG. 8: Comparison of the TMD functions in the HSO approach and their large- k_T behaviour predicted by pQCD. The bands show the variation of the TMD pdf of Eq. (28) (left) and the TMD ff Eq. (18) (right), with respect to mass parameters, using the Gaussian ansatzes of Eq. (43). The range of masses indicated in the labels are the same as those used to obtain the red band in the left panel of Fig. 6. The dot-dashed lines show the pQCD calculation of Eq. (42) for the TMD pdf (left), and that of Eq. (41) for the TMD ff (right). The correct behaviour for the models, has been imposed from the onset in Eq. (41) Eq. (42), through the A and B coefficients. This is indeed a necessary condition for the agreement of the TMD cross section and the asymptotic term in the left panel of Fig. 6.

transverse momentum perturbative tails. Such analyses can then be related directly to specific regions of observable transverse momentum in experimental data, in the spirit of, for example, the discussion of Fig. 17 in [8]. Ultimately, one hopes to infer, from the extracted correlation functions, information about the underlying nonperturbative physics. To see an example of where this will be useful, consider Ref. [85], which describes a treatment of intrinsic transverse momentum in a field theoretic chiral constituent quark model where the chiral symmetry breaking scale is large relative to the constituent quark mass. The HSO approach discussed in this paper is ideally suited for connecting this and similar descriptions to SIDIS data in the context of a complete TMD factorization treatment. Notice in particular that the additive model we constructed in Secs. (III)–(IV) aligns naturally with the Gaussian-plus-tail type of description in Ref. [85]. More generally, adopting an HSO approach enables us to begin to ask more specific and detailed phenomenological questions about the adequacy of specific theories of nonperturbative small transverse momentum behavior.

The elements necessary for these and other studies designed to identify separate perturbative and nonperturbative structures are in place now, and extensions to higher orders in α_s are straightforward, given existing results in the literature.

Acknowledgments

We thank Fatma Aslan, Mariaelena Boglione, Nobuo Sato, and Andrea Simonelli for useful conversations. J.O. Gonzalez-Hernandez acknowledges funding from the European Union’s Horizon 2020 research and innovation programme under grant agreement No 824093. T. Rogers and T. Rainaldi were supported by the U.S. Department of Energy, Office of Science, Office of Nuclear Physics, under Award Number DE-SC0018106. This work was also supported by the DOE Contract No. DE-AC05-06OR23177, under which Jefferson Science Associates, LLC operates Jefferson Lab.

Appendix A: Scale transformation function

The scale transition function in Eq. (39) is in principle entirely arbitrary, see the discussion in Sec. V of [16], provided it has the general feature that it transitions from $\sim 1/b_T$ behavior to Q_0 at a b_T slightly below $1/Q_0$. This ensures, by construction, that we avoid modifying the input scale treatment of Eq. (15) in the $Q \approx Q_0$ region. In this paper, namely in Fig. 5, we have adopted the same choice as in Appendix C of [16],

$$\bar{Q}_0(b_T, a) = Q_0 \left[1 - \left(1 - \frac{C_1}{Q_0 b_T} \right) e^{-b_T^2 a^2} \right]. \quad (\text{A1})$$

The constant C_1 has the usual numerical value of $C_1 = 2e^{-\gamma_E} \approx 1.123$. The specific value of a used in Fig. 5 is $a = Q_0$.

Appendix B: TMD parametrization in b_T space at the input scale

Here we list the b_T -space versions of Eq. (18) and Eq. (28)

$$\begin{aligned} z^2 \tilde{D}_{\text{inpt},h/j}(z, \mathbf{b}_T; \mu_{Q_0}, Q_0^2) &= K_0 (b_T m_{D_{h,j}}) \left[A_{h/j}^D(z; \mu_{Q_0}) + B_{h/j}^D(z; \mu_{Q_0}) \ln \left(\frac{b_T Q_0^2 e^{\gamma_E}}{2m_{D_{h,j}}} \right) \right] \\ &+ K_0 (b_T m_{D_{h,j}}) A_{h/j}^{D,g}(z; \mu_{Q_0}) \\ &+ C_{h/j}^D z^2 \tilde{D}_{\text{core},h/j}(z, \mathbf{b}_T; Q_0^2), \end{aligned} \quad (\text{B1})$$

$$\begin{aligned} \tilde{f}_{\text{inpt},i/p}(x, \mathbf{b}_T; \mu_{Q_0}, Q_0^2) &= K_0 (b_T m_{f_{i,p}}) \left[A_{i/p}^f(x; \mu_{Q_0}) + B_{i/p}^f(x; \mu_{Q_0}) \ln \left(\frac{b_T Q_0^2 e^{\gamma_E}}{2m_{f_{i,p}}} \right) \right] \\ &+ K_0 (b_T m_{f_{g,p}}) A_{g/p}^f(x; \mu_{Q_0}) \\ &+ C_{i/p}^f \tilde{f}_{\text{core},i/p}(x, \mathbf{b}_T; Q_0^2), \end{aligned} \quad (\text{B2})$$

where

$$\tilde{f}_{\text{core},i/p}(x, \mathbf{b}_T; Q_0^2) = \int d^2 \mathbf{k}_T e^{-i\mathbf{k}_T \cdot \mathbf{b}_T} f_{\text{core},i/p}(x, \mathbf{k}_T; Q_0^2), \quad (\text{B3})$$

$$\tilde{D}_{\text{core},h/j}(x, \mathbf{b}_T; Q_0^2) = \int d^2 \mathbf{k}_T e^{i\mathbf{k}_T \cdot \mathbf{b}_T} D_{\text{core},h/j}(x, z\mathbf{k}_T; Q_0^2), \quad (\text{B4})$$

which for the Gaussian and spectator model that we use read

$$\tilde{f}_{\text{core},i/p}^{\text{Gauss}}(x, \mathbf{b}_T; Q_0^2) = e^{-\frac{b_T^2 M_F^2}{4}}, \quad (\text{B5})$$

$$z^2 \tilde{D}_{\text{core},h/j}^{\text{Gauss}}(z, \mathbf{b}_T; Q_0^2) = e^{-\frac{b_T^2 M_D^2}{4z^2}}, \quad (\text{B6})$$

$$\tilde{f}_{\text{core},i/p}^{\text{Spect}}(x, \mathbf{b}_T; Q_0^2) = \frac{M_{0F}^2 (b_T M_{0F})^2}{4(2M_F^2 + M_{0F}^2)} \left(6K_2(b_T M_{0F}) + \frac{(M_F^2 - M_{0F}^2)(b_T M_{0F})}{M_{0F}^2} K_3(b_T M_{0F}) \right), \quad (\text{B7})$$

$$z^2 \tilde{D}_{\text{core},h/j}^{\text{Spect}}(z, \mathbf{b}_T; Q_0^2) = \frac{M_{0D}^2 (b_T M_{0D})}{2z^2 (M_D^2 + M_{0D}^2)} \left(4zK_1\left(\frac{b_T M_{0D}}{z}\right) + \frac{(M_D^2 - M_{0D}^2)(b_T M_{0D})}{M_{0D}^2} K_2\left(\frac{b_T M_{0D}}{z}\right) \right). \quad (\text{B8})$$

-
- [1] J. C. Collins and D. E. Soper, Nucl. Phys. **B193**, 381 (1981), erratum: **B213**, 545 (1983).
 - [2] J. C. Collins, D. E. Soper, and G. Sterman, Nucl. Phys. **B250**, 199 (1985).
 - [3] J. C. Collins, *Foundations of Perturbative QCD* (Cambridge University Press, Cambridge, 2011).
 - [4] R. Angeles-Martinez et al., Acta Phys. Polon. B **46**, 2501 (2015), 1507.05267.
 - [5] M. Anselmino, M. Guidal, and P. Rossi, *Topical issue on the 3-d structure of the nucleon* (2016).
 - [6] H. Gao, T. Liu, and Z. Zhao, PoS **DIS2018**, 232 (2018).

- [7] A. Bressan (COMPASS), PoS **QCDEV2017**, 009 (2018).
- [8] M. Aghasyan et al. (COMPASS), Phys. Rev. D **97**, 032006 (2018), 1709.07374.
- [9] M. Anselmino, M. Boglione, A. Prokudin, and C. Turk, Eur. Phys. J. **A31**, 373 (2007), hep-ph/0606286.
- [10] M. Boglione, J. O. G. Hernandez, S. Melis, and A. Prokudin, JHEP **02**, 095 (2015), 1412.1383.
- [11] P. Nadolsky, D. R. Stump, and C. P. Yuan, Phys. Rev. **D61**, 014003 (1999), hep-ph/9906280.
- [12] M. G. Echevarria, T. Kasemets, J.-P. Lansberg, C. Pisano, and A. Signori, Phys. Lett. **B781**, 161 (2018), 1801.01480.
- [13] E. Moffat, T. C. Rogers, N. Sato, and A. Signori, Phys. Rev. D **100**, 094014 (2019), 1909.02951.
- [14] A. Bacchetta, G. Bozzi, M. Lambertsen, F. Piacenza, J. Steiglechner, and W. Vogelsang, Phys. Rev. D **100**, 014018 (2019), 1901.06916.
- [15] P. B. Arnold and R. P. Kauffman, Nucl. Phys. **B349**, 381 (1991).
- [16] J. O. Gonzalez-Hernandez, T. C. Rogers, and N. Sato, Phys. Rev. D **106**, 034002 (2022), 2205.05750.
- [17] J. Arrington et al. (2021), 2112.00060.
- [18] J. Qiu and X.-F. Zhang, Phys. Rev. **D63**, 114011 (2001), hep-ph/0012348.
- [19] M. Grewal, Z.-B. Kang, J.-W. Qiu, and A. Signori, Phys. Rev. D **101**, 114023 (2020), 2003.07453.
- [20] M. Boglione, A. Dotson, L. Gamberg, S. Gordon, J. O. Gonzalez-Hernandez, A. Prokudin, T. C. Rogers, and N. Sato, JHEP **10**, 122 (2019), 1904.12882.
- [21] J. Collins and T. C. Rogers, Phys. Rev. D **96**, 054011 (2017), 1705.07167.
- [22] M. Schlemmer, A. Vladimirov, C. Zimmermann, M. Engelhardt, and A. Schäfer, JHEP **08**, 004 (2021), 2103.16991.
- [23] Y. Li et al., Phys. Rev. Lett. **128**, 062002 (2022), 2106.13027.
- [24] P. Shanahan, M. Wagman, and Y. Zhao, Phys. Rev. D **104**, 114502 (2021), 2107.11930.
- [25] M.-H. Chu et al. (LPC), Phys. Rev. D **106**, 034509 (2022), 2204.00200.
- [26] A. Kotzinian, Nucl. Phys. **B441**, 234 (1995), hep-ph/9412283.
- [27] L. P. Gamberg, G. R. Goldstein, and K. A. Oganessyan, Phys. Rev. D **67**, 071504 (2003), hep-ph/0301018.
- [28] A. Bacchetta, F. Conti, and M. Radici, Phys. Rev. D **78**, 074010 (2008), 0807.0323.
- [29] Z.-B. Kang, J.-W. Qiu, and H. Zhang, Phys. Rev. D **81**, 114030 (2010), 1004.4183.
- [30] J. V. Guerrero and A. Accardi (2020), 2010.07339.
- [31] B. Pasquini, S. Cazzaniga, and S. Boffi, Phys. Rev. D **78**, 034025 (2008), 0806.2298.
- [32] B. Pasquini and P. Schweitzer, Phys. Rev. D **83**, 114044 (2011), 1103.5977.
- [33] A. Bacchetta, S. Cotogno, and B. Pasquini, Phys. Lett. B **771**, 546 (2017), 1703.07669.
- [34] B. Pasquini and P. Schweitzer, Phys. Rev. D **90**, 014050 (2014), 1406.2056.
- [35] Z. Hu, S. Xu, C. Mondal, X. Zhao, and J. P. Vary (2022), 2205.04714.
- [36] S. Sakai, Prog. Theor. Phys. **63**, 1815 (1980).
- [37] S. Sakai, Prog. Theor. Phys. **63**, 1311 (1980).
- [38] F. Yuan, Phys. Lett. B **575**, 45 (2003), hep-ph/0308157.
- [39] H. Avakian, A. V. Efremov, P. Schweitzer, and F. Yuan, Phys. Rev. D **81**, 074035 (2010), 1001.5467.
- [40] A. I. Signal and F. G. Cao, Phys. Lett. B **826**, 136898 (2022), 2108.12116.
- [41] H. H. Matevosyan, W. Bentz, I. C. Cloet, and A. W. Thomas, Phys. Rev. D **85**, 014021 (2012), 1111.1740.
- [42] H. H. Matevosyan, A. W. Thomas, and W. Bentz, Phys. Rev. D **86**, 034025 (2012), 1205.5813.
- [43] S. Noguera and S. Scopetta, JHEP **11**, 102 (2015), 1508.01061.
- [44] C. Shi and I. C. Cloët, Phys. Rev. Lett. **122**, 082301 (2019), 1806.04799.
- [45] W. Broniowski and E. Ruiz Arriola, Phys. Lett. B **773**, 385 (2017), 1707.09588.
- [46] S. Bastami, L. Gamberg, B. Parsamyan, B. Pasquini, A. Prokudin, and P. Schweitzer, JHEP **02**, 166 (2021), 2005.14322.
- [47] S. Bastami, A. V. Efremov, P. Schweitzer, O. V. Teryaev, and P. Zavada, Phys. Rev. D **103**, 014024 (2021), 2011.06203.
- [48] P. Schweitzer, T. Teckentrup, and A. Metz, Phys. Rev. **D81**, 094019 (2010), 1003.2190.
- [49] M. Anselmino, M. Boglione, U. D'Alesio, S. Melis, F. Murgia, et al., Phys. Rev. **D87**, 094019 (2013), 1303.3822.
- [50] M. Anselmino, M. Boglione, J. Gonzalez H., S. Melis, and A. Prokudin, JHEP **1404**, 005 (2014), arXiv:1312.6261.
- [51] A. Bacchetta, L. P. Gamberg, G. R. Goldstein, and A. Mukherjee, Phys. Lett. B **659**, 234 (2008), 0707.3372.
- [52] P. Aurenche, R. Basu, M. Fontannaz, and R. M. Godbole, Eur. Phys. J. C **34**, 277 (2004), hep-ph/0312359.
- [53] A. Daleo, D. de Florian, and R. Sassot, Phys. Rev. **D71**, 034013 (2005), hep-ph/0411212.
- [54] B. Wang, J. O. Gonzalez-Hernandez, T. C. Rogers, and N. Sato, Phys. Rev. D **99**, 094029 (2019), 1903.01529.
- [55] Y. Koike, J. Nagashima, and W. Vogelsang, Nucl. Phys. **B744**, 59 (2006), hep-ph/0602188.
- [56] J. Collins and T. Rogers, Phys. Rev. D **91**, 074020 (2015), 1412.3820.
- [57] T. C. Rogers, Eur. Phys. J. A **52**, 153 (2016), 1509.04766.
- [58] F. Aslan, L. Gamberg, J. O. Gonzalez-Hernandez, T. Rainaldi, and T. C. Rogers (2022), 2212.00757.
- [59] C. T. H. Davies, B. R. Webber, and W. J. Stirling, **1**, I.95 (1984).
- [60] C. Balázs, J. Qiu, and C. Yuan, Phys. Lett. **B355**, 548 (1995), hep-ph/9505203.
- [61] F. Landry, R. Brock, G. Ladinsky, and C. P. Yuan, Phys. Rev. **D63**, 013004 (2001), hep-ph/9905391.
- [62] P. Sun and F. Yuan, Phys. Rev. **D88**, 034016 (2013), 1304.5037.
- [63] P. Sun and F. Yuan, Phys. Rev. **D88**, 114012 (2013), 1308.5003.
- [64] M. Bury, F. Hautmann, S. Leal-Gomez, I. Scimemi, A. Vladimirov, and P. Zurita (2022), 2201.07114.
- [65] A. Bacchetta, V. Bertone, C. Bissolotti, G. Bozzi, M. Cerutti, F. Piacenza, M. Radici, and A. Signori (MAP), JHEP **10**, 127 (2022), 2206.07598.
- [66] P. M. Nadolsky, H.-L. Lai, Q.-H. Cao, J. Huston, J. Pumplin, D. Stump, W.-K. Tung, and C. P. Yuan, Phys. Rev. D **78**, 013004 (2008), 0802.0007.

- [67] R. A. Khalek, V. Bertone, and E. R. Nocera, *Phys. Rev. D* **104**, 034007 (2021), 2105.08725.
- [68] A. Buckley, J. Ferrando, S. Lloyd, K. Nordström, B. Page, M. Rüfenacht, M. Schönherr, and G. Watt, *Eur. Phys. J. C* **75**, 132 (2015), 1412.7420.
- [69] R. Abdul Khalek et al., *Nucl. Phys. A* **1026**, 122447 (2022), 2103.05419.
- [70] J. O. Gonzalez-Hernandez, T. C. Rogers, N. Sato, and B. Wang, *Phys. Rev. D* **98**, 114005 (2018), 1808.04396.
- [71] A. Bacchetta, D. Boer, M. Diehl, and P. J. Mulders, *JHEP* **08**, 023 (2008), 0803.0227.
- [72] J.-W. Qiu, T. C. Rogers, and B. Wang, *Phys. Rev. D* **101**, 116017 (2020), 2004.13193.
- [73] T. Rogers, *Mod. Phys. Lett. A* **35**, 2030021 (2020), 2008.05351.
- [74] M. A. Kimber, A. D. Martin, and M. G. Ryskin, *Phys. Rev.* **D63**, 114027 (2001), hep-ph/0101348.
- [75] G. Watt, A. D. Martin, and M. G. Ryskin, *Eur. Phys. J.* **C31**, 73 (2003), hep-ph/0306169.
- [76] B. Guiot, *Phys. Rev. D* **107**, 014015 (2023), 2205.02873.
- [77] K. Golec-Biernat and A. M. Stasto, *Phys. Lett. B* **781**, 633 (2018), 1803.06246.
- [78] B. Guiot, *Phys. Rev. D* **101**, 054006 (2020), 1910.09656.
- [79] S. Catani, D. de Florian, and M. Grazzini, *Nucl. Phys.* **B596**, 299 (2001), hep-ph/0008184.
- [80] S. Catani, L. Cieri, D. de Florian, G. Ferrera, and M. Grazzini, *Eur. Phys. J.* **C72**, 2195 (2012), 1209.0158.
- [81] S. Camarda et al., *Eur. Phys. J. C* **80**, 251 (2020), [Erratum: *Eur.Phys.J.C* 80, 440 (2020)], 1910.07049.
- [82] T. Becher, M. Neubert, and B. D. Pecjak, *JHEP* **01**, 076 (2007), hep-ph/0607228.
- [83] T. Becher and M. Neubert, *Eur. Phys. J.* **C71**, 1665 (2011), 1007.4005.
- [84] M. G. Echevarría, A. Idilbi, and I. Scimemi, *JHEP* **1207**, 002 (2012), 1111.4996.
- [85] P. Schweitzer, M. Strikman, and C. Weiss, *JHEP* **1301**, 163 (2013), 1210.1267.